

---

# System-Embedded Diffusion Bridge Models

---

Bartłomiej Sobieski<sup>\*†1</sup>, Matthew Tivnan<sup>†2,3</sup>, Yuang Wang<sup>2,3</sup>, Siyeop Yoon<sup>2,3</sup>,  
Pengfei Jin<sup>2,3</sup>, Dufan Wu<sup>2,3</sup>, Quanzheng Li<sup>2,3</sup>, Przemyslaw Biecek<sup>1,4</sup>

<sup>1</sup>University of Warsaw, <sup>2</sup>Harvard University,

<sup>3</sup>Massachusetts General Hospital, <sup>4</sup>Warsaw University of Technology

## Abstract

Solving inverse problems—recovering signals from incomplete or noisy measurements—is fundamental in science and engineering. Score-based generative models (SGMs) have recently emerged as a powerful framework for this task. Two main paradigms have formed: unsupervised approaches that adapt pretrained generative models to inverse problems, and supervised bridge methods that train stochastic processes conditioned on paired clean and corrupted data. While the former typically assume knowledge of the measurement model, the latter have largely overlooked this structural information. We introduce System-embedded Diffusion Bridge Models (SDBs), a new class of supervised bridge methods that explicitly embed the known linear measurement system into the coefficients of a matrix-valued SDE. This principled integration yields consistent improvements across diverse linear inverse problems and demonstrates robust generalization under system misspecification between training and deployment, offering a promising solution to real-world applications.

## 1 Introduction

Restoring data from corrupted or incomplete measurements is a fundamental task in science and engineering [Abbott et al., 2016, Akiyama et al., 2019], commonly referred to as an *inverse problem*. Its *linear* formulation plays a central role in practical domains such as signal processing and medical imaging [Bertero et al., 1985, Candes et al., 2006]. The emergence of deep learning has significantly advanced this field, enabling major scientific breakthroughs [Ongie et al., 2020]. Since the work of Song et al. [2021b], the scientific community has increasingly adopted *score-based generative models* (SGMs), also known as *diffusion models*, to tackle inverse problems. Two key directions have emerged: one adapts models pretrained for image synthesis to conditional generation; the other, often called *bridge methods*, trains problem-specific models grounded in stochastic differential equations (SDEs), assuming access to paired samples of clean data and corresponding measurements.

While pretrained models often assume access to a known linear measurement system, bridge methods have primarily focused on developing general-purpose approaches without leveraging such structural information. However, in many real-world settings—such as CT or MRI reconstruction—the linear measurement process is known *a priori*, and datasets frequently contain paired examples of clean and degraded data.

To address this gap, we propose *System-embedded Diffusion Bridge Models* (SDBs), a novel method that incorporates the system response and noise covariance directly into the coefficients of a matrix-valued SDE. By embedding this measurement-system knowledge, SDB achieves considerable performance gains across diverse linear systems of varying complexity, demonstrated through three distinct instantiations. Furthermore, we conduct an extensive study of SDB’s generalization under system misspecification between training and deployment, showing that SDB consistently outperforms baselines and remains robust in the face of parameter shifts, making it well-suited for real-world deployment.

---

\*Corresponding author at b.sobieski@uw.edu.pl

†Equal contribution

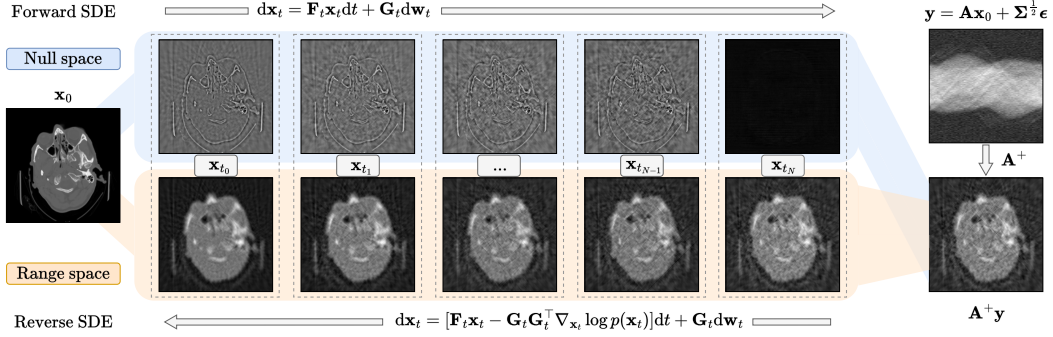


Figure 1: SDB learns a diffusion bridge between pseudoinverse reconstructions and clean samples by embedding the measurement system into the coefficients of the linear SDE, allowing the score model to distinguish between the range and null spaces of the task.

In addition, our work advocates for more expressive formulations of diffusion processes in generative modeling, opening avenues for future research into system-aware and structure-driven stochastic modeling frameworks.<sup>3</sup>

## 2 Related works

Our work offers a new perspective on constructing task-specific diffusion bridges (*supervised*), while drawing inspiration from diffusion-based plug-and-play methods (*unsupervised*). Both directions address the topic of image restoration and inverse problems from different viewpoints. Below, we briefly cover these directions, with a much more detailed overview included in the Appendix.

**Diffusion models for inverse problems.** As shown in the work of Song et al. [2021b], pretrained unconditional diffusion models can be easily adapted to conditional synthesis with a simple application of Bayes’ Theorem. The resulting likelihood term has been extensively utilized for guided generation [Dhariwal and Nichol, 2021], especially for image restoration problems [Daras et al., 2024]. These methods range from generic ones [Song et al., 2021b, Chung et al., 2022] to those that incorporate additional assumptions and constraints to the generation process, such as DPS [Chung et al., 2023a], DDNM [Wang et al., 2023], IIGDM [Song et al., 2023a], DDPG [Garber and Tirer, 2024], and others [Kawar et al., 2022, Chung et al., 2022, 2023a, Song et al., 2023a, Mardani et al., 2024, Chung et al., 2024].

**Diffusion bridges.** One may also extend the SGM framework to arrive at mappings between arbitrary probability distributions given paired data [Särkkä and Solin, 2019]. Among many seminal works in this area [Heng et al., 2021, Somnath et al., 2023, Peluchetti, 2022, Delbracio and Milanfar, 2023, De Bortoli et al., 2021], Liu et al. [2023] (I2SB) propose a simulation-free algorithm that solves the Schrödinger Bridge (SB) problem, Luo et al. [2023a] (IR-SDE) construct a conditional stochastic differential equation (SDE) that maps noisy degradations to clean samples, while Yue et al. [2024] (GOUB) generalize it with the Doob’s h-transform [Doob, 1984], which is also used by Zhou et al. [2024] (DDBM) to generalize the entire SGM framework.

## 3 Background

**Diffusion models.** Generative modeling of visual data has advanced rapidly with the introduction of diffusion models [Sohl-Dickstein et al., 2015, Ho et al., 2020, Dhariwal and Nichol, 2021], which generate images by sequential denoising. Initially formulated as a discrete Markov chain with Gaussian kernels, diffusion models were later unified with score matching [Song and Ermon, 2019] under the framework of SDEs [Song et al., 2021b], establishing the continuous-time formulation known as SGM.

<sup>3</sup>We include the source code at <https://github.com/sobieski/sdb>.

Let  $p(\mathbf{x}_t)$  denote the probability distribution of  $\mathbf{x}_t \in \mathbb{R}^d$  parameterized by time  $t \in [0, 1]$ , where  $p(\mathbf{x}_0)$  represents the data distribution and  $p(\mathbf{x}_1)$  the prior. In this work, we highlight the often-overlooked *linear* formulation of SGM. The forward SDE, which maps  $p(\mathbf{x}_0)$  to  $p(\mathbf{x}_1)$ , is defined as

$$d\mathbf{x}_t = \mathbf{F}_t \mathbf{x}_t dt + \mathbf{G}_t d\mathbf{w}_t, \quad (1)$$

where  $\mathbf{F}_t \mathbf{x}_t$  is a linear drift term with time-dependent matrix  $\mathbf{F}_t \in \mathbb{R}^{d \times d}$ , and  $\mathbf{G}_t$  is a matrix-valued diffusion coefficient. Following Anderson [1982], the reverse SDE, which maps  $p(\mathbf{x}_1)$  to  $p(\mathbf{x}_0)$ , is given by

$$d\mathbf{x}_t = [\mathbf{F}_t \mathbf{x}_t - \mathbf{G}_t \mathbf{G}_t^\top \nabla_{\mathbf{x}_t} \log p(\mathbf{x}_t)] dt + \mathbf{G}_t d\bar{\mathbf{w}}_t, \quad (2)$$

where  $\nabla_{\mathbf{x}_t} \log p(\mathbf{x}_t)$  is the score function and  $\bar{\mathbf{w}}_t$  is the Wiener process with reversed time. The forward-reverse relationship ensures that the marginal distributions  $p(\mathbf{x}_t)$ , defined by eq. (1) and eq. (2), remain consistent.

In standard SGM for image synthesis,  $p(\mathbf{x}_1)$  is typically chosen as an isotropic Gaussian. To generate samples from  $p(\mathbf{x}_0)$ , one samples from  $p(\mathbf{x}_1)$  and solves eq. (2) using a time discretization scheme. This requires the unknown score function  $\nabla_{\mathbf{x}_t} \log p(\mathbf{x}_t)$ , which is generally approximated by a neural network  $\mathbf{s}_\theta(\mathbf{x}_t, t)$  trained with the score-matching loss [Song et al., 2021b]:

$$\mathbb{E}[\|\mathbf{s}_\theta(\mathbf{x}_t, t) - \nabla_{\mathbf{x}_t} \log p(\mathbf{x}_t | \mathbf{x}_0)\|_2^2], \quad (3)$$

where the expectation is taken over  $\mathbf{x}_0 \sim p(\mathbf{x}_0)$ ,  $t \sim \mathcal{U}([0, 1])$ , and  $\mathbf{x}_t \sim p(\mathbf{x}_t | \mathbf{x}_0)$ .

The linear formulation in eq. (1) and eq. (2) is a special case of the broader SGM framework introduced by Song et al. [2021b], where drift and diffusion coefficients can be arbitrarily complex functions of  $\mathbf{x}_t$  and  $t$ . This linear formulation, however, generalizes the well-established *scalar* case. Specifically, the Variance-Preserving (VP) SDE, which maintains constant variance for  $\mathbf{x}_t$  across time, can be recovered with  $\mathbf{F}_t = -\frac{1}{2}\beta_t \mathbf{I}$  and  $\mathbf{G}_t = \sqrt{\beta_t} \mathbf{I}$ . The Variance-Exploding (VE) SDE, which induces unbounded growth in the variance of  $p(\mathbf{x}_1)$  as  $t \rightarrow 1$ , is obtained with  $\mathbf{F}_t = \mathbf{0}$  and  $\mathbf{G}_t = \sqrt{\frac{d\sigma_t^2}{dt}} \mathbf{I}$ . While these scalar matrices offer simplicity, they also raise the question of whether more sophisticated designs could yield additional benefits.

**Inverse problems.** For a signal sample  $\mathbf{x} \in \mathbb{R}^d$ , we define the *linear measurement system* as

$$\mathbf{y} = \mathbf{A}\mathbf{x} + \Sigma^{\frac{1}{2}} \boldsymbol{\epsilon}, \quad (4)$$

where  $\mathbf{y} \in \mathbb{R}^m$  is the *measurement*,  $\mathbf{A} \in \mathbb{R}^{m \times d}$  is the *system response matrix*,  $\boldsymbol{\epsilon} \sim \mathcal{N}(\mathbf{0}_m, \mathbf{I}_{m \times m})$  is the measurement noise with covariance matrix  $\Sigma \in \mathbb{R}^{m \times m}$  and  $p(\mathbf{y} | \mathbf{x}) = \mathcal{N}(\mathbf{A}\mathbf{x}, \Sigma)$  is the *forward model*. We refer to finding the unknown  $\mathbf{x}$  based on the provided  $\mathbf{y}$  as solving a linear inverse problem with additive Gaussian noise [Tarantola, 2005]. This formulation is central to many practical applications, such as signal processing, medical imaging, and remote sensing [Mueller and Siltanen, 2012], particularly in the case of noninvertible linear systems, where either  $m \neq d$  or  $\mathbf{A}$  is rank-deficient.

**Matrix pseudoinverse.** Consider the simplest noiseless ( $\Sigma = \mathbf{0}_{m \times m}$ ) setting of eq. (4) with invertible  $\mathbf{A}$ . In this case, the original signal  $\mathbf{x}$  can be fully recovered by simply using the inverse of  $\mathbf{A}$ , *i.e.*,  $\mathbf{x} = \mathbf{A}^{-1}\mathbf{y}$ . However, this is only possible when  $m = d$  and  $\mathbf{A}$  is full-rank, which greatly limits the scope of potential inverse problems. In practice, the matrix  $\mathbf{A}$  is typically not invertible, and noise arises naturally due to, *e.g.*, imperfections in the measurement process.

In the case of non-invertible  $\mathbf{A}$ , one may utilize its Moore-Penrose inverse, often called the *pseudoinverse*, denoted as  $\mathbf{A}^+$ . It generalizes the notion of standard inverse of square matrices to those of arbitrary shape and rank. Consider the singular value decomposition (SVD)  $\mathbf{A} = \mathbf{U}\mathbf{D}\mathbf{V}^*$  of  $\mathbf{A}$  for matrices  $\mathbf{U}, \mathbf{D}, \mathbf{V}$ , where  $\mathbf{U}$  and  $\mathbf{V}$  are unitary, and  $\mathbf{D}$  is diagonal with non-negative real entries. Then, its pseudoinverse is computed via  $\mathbf{A}^+ = \mathbf{V}\mathbf{D}^+\mathbf{U}^*$ , where  $\mathbf{D}^+$  is obtained by replacing all of its non-zero singular values with their reciprocals.

**Range-nullspace decomposition.** A particularly useful property of the matrix pseudoinverse is its role in the well-known range-nullspace decomposition [Strang, 2022]. Specifically, any signal  $\mathbf{x}$  can be decomposed as

$$\mathbf{x} = \underbrace{\mathbf{A}^+ \mathbf{A} \mathbf{x}}_{\text{range space}} + \underbrace{(\mathbf{I} - \mathbf{A}^+ \mathbf{A}) \mathbf{x}}_{\text{null space}}, \quad (5)$$

where the first term lies in the range (image) of  $\mathbf{A}$ , and the second in its null space (kernel), *i.e.*, it is annihilated by  $\mathbf{A}$ . This decomposition is particularly relevant in inverse problems: applying  $\mathbf{A}$  to  $\mathbf{x}$  eliminates the null space component, while preserving the range component. Consequently, solving an inverse problem can be viewed as denoising in the range space and synthesizing missing information in the null space.

**Pseudoinverse reconstruction.** A matrix pseudoinverse can also be used to compute the *pseudoinverse reconstruction* (PR)  $\hat{\mathbf{x}}$  of  $\mathbf{x}$  via  $\hat{\mathbf{x}} = \mathbf{A}^+\mathbf{y}$ . Crucially, this reconstruction always lies in  $\mathbb{R}^d$ , regardless of the shape of  $\mathbf{y}$ . This property addresses a common limitation of prior bridge methods, *i.e.*, their default operation in fixed-dimensional spaces. When  $m \neq d$ , such methods require additional effort to remain well-defined. For more challenging inverse problems, such as those in medical imaging, PR provides a principled mechanism for resolving this issue.

From a theoretical perspective, assuming access to  $\mathbf{A}^+$  also simplifies the relationship between  $\mathbf{x}$  and  $\mathbf{y}$  [Strang, 2022]. When  $m < d$ , the PR is the unique minimizer of  $\|\mathbf{A}\mathbf{x}^* - \mathbf{y}\|_2$  over all  $\mathbf{x}^* \in \mathbb{R}^d$ . When  $m > d$ , it yields the minimum  $\ell_2$ -norm solution among those satisfying  $\mathbf{A}\mathbf{x}^* = \mathbf{y}$ , *i.e.*,  $\min_{\mathbf{x}^*} \|\mathbf{x}^*\|_2$  subject to  $\mathbf{A}\mathbf{x}^* = \mathbf{y}$ . These optimality properties further motivate the use of PR when  $\mathbf{A}$  is known and its pseudoinverse is tractable.

**Problem-specific diffusion bridges.** Many unsupervised approaches, assuming access to a specific noisy linear system (eq. (4)), offer tailored solutions that improve performance under additional assumptions [Song et al., 2023a, Wang et al., 2023, Chung et al., 2023a, Garber and Tirer, 2024]. In contrast, state-of-the-art (SOTA) diffusion bridges [Liu et al., 2023, Luo et al., 2023a, Yue et al., 2024, Zhou et al., 2024] make no assumptions about the underlying system during training, focusing on general mappings between arbitrary distributions. This can be suboptimal when the system is (even approximately) known. For instance, in image inpainting, these methods do not distinguish between the known range (unmasked) and the missing null part (masked), resulting in redundant noise in the range space, which is expected to be noiseless. In more complex scenarios, such redundancy could reduce efficiency, while ignoring system-specific information may hinder generalization. Thus, developing a supervised diffusion bridge tailored to a specific system remains an important yet unresolved challenge.

## 4 Method

In this section, we seek to construct a bridge diffusion process that directly incorporates the information about the assumed measurement system. By that, we understand a process which i) maps the PRs to the respective signal samples, ii) synthesizes the missing information directly in the null space and iii) optionally denoises the range space part. We begin by noticing a specific connection between how intermediate steps of a general linear diffusion process are obtained and how noisy linear measurement systems map clean samples to observations. As our key contribution, we propose a specific design of matrix-valued SDEs, which fulfill the initially desired properties.

**Connecting systems to SDEs.** Following eq. (4), it is clear that  $\mathbf{y} \mid \mathbf{x} \sim \mathcal{N}(\mathbf{A}\mathbf{x}, \Sigma)$ , *i.e.*, for a given signal  $\mathbf{x}$ , a noisy linear system applies a linear transformation  $\mathbf{A}$  and adds (possibly correlated) Gaussian noise to sample a measurement. On the other hand, given a clean sample  $\mathbf{x}_0$ , eq. (1) transforms it to  $\mathbf{x}_t$  by applying a *cascade* of such noisy linear systems, which is a noisy linear system itself. That is,  $\mathbf{x}_t \mid \mathbf{x}_0 \sim \mathcal{N}(\mathbf{H}_t\mathbf{x}_0, \Sigma_t)$  for some time-dependent matrices  $\mathbf{H}_t, \Sigma_t$ . Hence, one may equivalently arrive at  $\mathbf{y} \mid \mathbf{x}$  (or some linear transformation of  $\mathbf{y}$ ) through an application of a series of noisy linear systems to  $\mathbf{x}$  instead of just a single one. In the limit, this would imply the existence of a general linear SDE that performs such mapping.

The above considerations suggest that the measurement system could be directly *embedded* into  $\mathbf{H}_t$  and  $\Sigma_t$  to arrive at such SDE. While the relationship between these and the drift and diffusion coefficients of the corresponding stochastic process is not immediately clear, a recent theoretical result derived by Tivnan et al. [2025] provides a convenient way of mapping from one to the other under mild assumptions. We restate it below for clarity.

**Theorem 1** [Tivnan et al., 2025] Assume that  $\mathbf{x}_t | \mathbf{x}_0$  evolves according to the linear forward process from eq. (1). Then,  $\mathbf{x}_t | \mathbf{x}_0 \sim \mathcal{N}(\mathbf{H}_t \mathbf{x}_0, \mathbf{\Sigma}_t)$ , where

$$\mathbf{H}_t = \exp(\mathbf{\Omega}_t(\mathbf{F}_t)) \approx \exp\left(\int_0^t \mathbf{F}_s ds\right), \mathbf{\Sigma}_t = \mathbf{H}_t \left(\int_0^t \mathbf{H}_s^{-1} \mathbf{G}_s \mathbf{G}_s^\top \mathbf{H}_s^{-1\top} ds\right) \mathbf{H}_t^\top, \quad (6)$$

where  $\mathbf{\Omega}_t$  is the Magnus expansion and the approximation becomes equality if, for all  $s, s' \in [0, t]$ ,  $[\mathbf{F}_s, \mathbf{F}_{s'}] = 0$ , i.e.,  $\mathbf{F}_s$  and  $\mathbf{F}_{s'}$  commute. Conversely, given  $\mathbf{H}_t$  and  $\mathbf{\Sigma}_t$ , the drift and diffusion coefficients can be obtained via:

$$\mathbf{F}_t = \frac{d\mathbf{H}_t}{dt} \mathbf{H}_t^{-1}, \mathbf{G}_t \mathbf{G}_t^\top = \frac{d\mathbf{\Sigma}_t}{dt} - \mathbf{F}_t \mathbf{\Sigma}_t - \mathbf{\Sigma}_t \mathbf{F}_t^\top. \quad (7)$$

Therefore, theorem 1 allows one to obtain the linear diffusion process governing the evolution of  $\mathbf{x}_t | \mathbf{x}_0$  defined through  $\mathbf{H}_t$  and  $\mathbf{\Sigma}_t$ , which in turn makes training and sampling from continuous-time models possible.

**Embedding the measurement system.** Equipped with the necessary tools, we propose to embed the measurement system into the linear diffusion process by using

$$\mathbf{H}_t = \mathbf{A}^+ \mathbf{A} + \alpha_t (\mathbf{I} - \mathbf{A}^+ \mathbf{A}), \quad (8a)$$

$$\mathbf{\Sigma}_t = \gamma_t \mathbf{A}^+ \mathbf{\Sigma} \mathbf{A}^{+\top} + \beta_t (\mathbf{I} - \mathbf{A}^+ \mathbf{A}). \quad (8b)$$

for  $\alpha_t, \beta_t, \gamma_t$  being the null space drift, null space diffusion and range space diffusion coefficients respectively. We refer to the process resulting from eqs. (8a) and (8b) as the *System-embedded Diffusion Bridge Model* (SDB).

To better understand the rationale behind this specific design, it is worth considering the range and null space components of the resulting  $\mathbf{x}_t$  separately. Specifically,

$$\mathbf{A}^+ \mathbf{A} \mathbf{x}_t = \mathbf{A}^+ (\mathbf{A} \mathbf{x}_0 + \gamma_t \mathbf{\Sigma}^{\frac{1}{2}} \epsilon) = \mathbf{A}^+ \mathbf{A} \mathbf{x}_0 + \gamma_t \mathbf{A}^+ \mathbf{\Sigma}^{\frac{1}{2}} \epsilon, \quad (9a)$$

$$(\mathbf{I} - \mathbf{A}^+ \mathbf{A}) \mathbf{x}_t = \alpha_t (\mathbf{I} - \mathbf{A}^+ \mathbf{A}) \mathbf{x}_0 + \beta_t (\mathbf{I} - \mathbf{A}^+ \mathbf{A}) \epsilon', \quad (9b)$$

where  $\epsilon \sim \mathcal{N}(\mathbf{0}_m, \mathbf{\Sigma}_{m \times m})$ ,  $\epsilon' \sim \mathcal{N}(\mathbf{0}_d, \mathbf{\Sigma}_{d \times d})$ . The range space part contains the original signal  $\mathbf{A}^+ \mathbf{A} \mathbf{x}_0$  and the stochastic component  $\gamma_t \mathbf{A}^+ \mathbf{\Sigma}^{\frac{1}{2}} \epsilon$ , which directly models the range space noise. If  $\mathbf{\Sigma} = \mathbf{0}$ , the true signal is fully recovered at every timestep  $t$ . The null space part is a mixture of the null component of the true signal  $\alpha_t (\mathbf{I} - \mathbf{A}^+ \mathbf{A}) \mathbf{x}_0$  and null-space-projected Gaussian noise  $\beta_t (\mathbf{I} - \mathbf{A}^+ \mathbf{A}) \epsilon'$ . Notably, SDB links two stochastic processes that evolve simultaneously within the range and null spaces, each modeled with independent noise variables,  $\epsilon$  and  $\epsilon'$ . Moreover, it is evident that proper choices for  $\alpha_t, \beta_t$  and  $\gamma_t$  lead to a mapping between the PRs at  $t = 1$  to their respective clean samples at  $t = 0$ .

**SDE perspective.** Applying theorem 1 to the coefficients from eq. (8) leads to the following drift and diffusion coefficients for SDB:

$$\mathbf{F}_t = \frac{d}{dt} \log \alpha_t (\mathbf{I} - \mathbf{A}^+ \mathbf{A}), \quad (10a)$$

$$\mathbf{G}_t \mathbf{G}_t^\top = \frac{d\gamma_t}{dt} \mathbf{A}^+ \mathbf{\Sigma} \mathbf{A}^{+\top} + \left( \frac{d\beta_t}{dt} - 2\beta_t \frac{d}{dt} \log \alpha_t \right) (\mathbf{I} - \mathbf{A}^+ \mathbf{A}). \quad (10b)$$

With this formulation at hand, we now propose a specific setting of the scalar functions  $\alpha_t$  and  $\beta_t$ , which extend the result of Liu et al. [2023] and make direct connection of SDB to the optimal transport (OT) plan [Mikami, 2004].

**Theorem 2** For the linear SDE defined in eq. (1) with  $\mathbf{F}_t$  and  $\mathbf{G}_t$  given by eqs. (10a) and (10b) respectively, let  $\alpha_t = \frac{\bar{\sigma}_t^2}{\bar{\sigma}_t^2 + \sigma_t^2}$ ,  $\beta_t = \frac{\sigma_t^2 \bar{\sigma}_t^2}{\bar{\sigma}_t^2 + \sigma_t^2}$  for  $\sigma_t^2 = \int_0^t g^2(\tau) d\tau$ ,  $\bar{\sigma}_t^2 = \int_t^1 g^2(\tau) d\tau$  for some non-negative function  $g(t)$ . Assuming that  $g(t) \rightarrow 0$  uniformly for all  $t$ , the null space part of this SDE reduces to an OT-ODE:

$$d(\mathbf{I} - \mathbf{A}^+ \mathbf{A}) \mathbf{x}_t = \mathbf{v}_t(\mathbf{x}_t | \mathbf{x}_0) dt, \quad (11)$$

where  $\mathbf{v}_t(\mathbf{x}_t | \mathbf{x}_0) = \left( \lim_{g(t) \rightarrow 0} \frac{g^2(t)}{\sigma_t^2} \right) (\mathbf{I} - \mathbf{A}^+ \mathbf{A}) (\mathbf{x}_t - \mathbf{x}_0)$ .

We include the proof in the Appendix. To align the dynamics between the range and null space, we also use  $\gamma_t = \frac{\sigma_t^2}{\bar{\sigma}_t^2 + \sigma_t^2}$ . In practice, we do not set  $g(t) = 0$ , but rather keep it at sufficiently low values. Because of the relationship to the SB problem, we term this variant as SDB (SB).

**Novel processes.** To showcase the versatility of our framework, we introduce two additional variants of SDB that reinterpret the VP and VE diffusion processes of Song et al. [2021b]:

$$\text{SDB (VP): } \alpha_t = 1 - t, \beta_t = \sqrt{1 - \alpha_t}, \gamma_t = \beta_t,$$

$$\text{SDB (VE): } \alpha_t = 1, \beta_t = \sigma_{max} \sqrt{t}, \gamma_t = \sqrt{t}, \text{ where } \sigma_{max} \gg 1.$$

In both cases, the original VP or VE process is applied in the null space, while the range space coefficient  $\gamma_t$  is related to  $\beta_t$  to simplify the dynamics. Unlike methods such as DDBM, which symmetrize the variance schedule around  $t = 0.5$ , these variants explicitly control how the original signal is erased in the null space. There, SDB (VP) performs a convex interpolation between the clean input and Gaussian noise, while SDB (VE) converges to an isotropic Gaussian  $\mathcal{N}(\mathbf{0}, \sigma_{max}^2 \mathbf{I})$  as  $t \rightarrow 1$ . As such, both more closely resemble approaches like IR-SDE that retain non-singular marginals at the endpoint. For simplicity, we parameterize SDB (VP) and SDB (VE) processes with linear scheduling, leaving more sophisticated designs as future work.

Additional technical details, including the chosen network parameterization and an extended discussion of nonlinear measurement systems, are provided in the Appendix.

Table 1: Comparison of prior SOTA diffusion bridge methods with SDB. Subsequent rows denote the drift ( $\mathbf{F}_t$ ) and diffusion ( $\mathbf{G}_t$ ) coefficients of the forward process, while  $\boldsymbol{\mu}_t, \boldsymbol{\Sigma}_t$  are its respective mean and covariance at timestep  $t$ . Each column follows the original notation of each paper.

Method	I2SB	IR-SDE	GOUB	DDBM (VP)	SDB (SB)
$\mathbf{F}_t$	$\frac{\beta_t}{\sigma_x^2 + \sigma_t^2}(\mathbf{x}_1 - \mathbf{x}_0) - \beta_t \frac{\sigma_x^2 - \sigma_t^2}{\sigma_x^2 \sigma_t^2}(\mathbf{x}_t - \boldsymbol{\mu}_t)$	$\theta_t(\mathbf{x}_1 - \mathbf{x}_t)$	$(\theta_t + g^2(t) \frac{e^{-2\theta_t t}}{\sigma_{t,1}^2})(\mathbf{x}_1 - \mathbf{x}_t)$	$(\frac{d}{dt} \log \alpha_t) \mathbf{x}_t + g^2(t) \frac{(\frac{\sigma_x}{\sigma_t} \mathbf{x}_1 - \mathbf{x}_t)}{\sigma_t^2 (\frac{\text{SNR}_t}{\text{SNR}_t - 1})}$	$\frac{d}{dt} \log \alpha_t (\mathbf{I} - \mathbf{A}^+ \mathbf{A})$
$\mathbf{G}_t \mathbf{G}_t^\top$	$\beta_t \mathbf{I}$	$\sigma^2(t) \mathbf{I}$	$g^2(t) \mathbf{I}$	$g^2(t) \mathbf{I}$	$(\frac{d\gamma_t}{dt}) \mathbf{A}^+ \boldsymbol{\Sigma} \mathbf{A}^{+\top} + (\frac{d\beta_t}{dt} - 2\beta_t \frac{d}{dt} \log \alpha_t) (\mathbf{I} - \mathbf{A}^+ \mathbf{A})$
$\boldsymbol{\mu}_t$	$\frac{\sigma_x^2}{\sigma_x^2 + \sigma_t^2} \mathbf{x}_0 + \frac{\sigma_t^2}{\sigma_x^2 + \sigma_t^2} \mathbf{x}_1$	$\mathbf{x}_1 + (\mathbf{x}_0 - \mathbf{x}_1) e^{-\bar{\theta}_t t}$	$e^{-\bar{\theta}_t t} \frac{\sigma_{t,1}^2}{\sigma_{t,1}^2} \mathbf{x}_0 + [(1 - e^{-\bar{\theta}_t t}) \frac{\sigma_{t,1}^2}{\sigma_{t,1}^2} + e^{-2\bar{\theta}_t t} \frac{\sigma_{t,1}^2}{\sigma_{t,1}^2}] \mathbf{x}_1$	$\frac{\text{SNR}_t \alpha_t}{\text{SNR}_t \alpha_t} \mathbf{x}_1 + \alpha_t (1 - \frac{\text{SNR}_t}{\text{SNR}_t}) \mathbf{x}_0$	$\mathbf{A}^+ \mathbf{A} \mathbf{x}_0 + \alpha_t (\mathbf{I} - \mathbf{A}^+ \mathbf{A}) \mathbf{x}_0$
$\boldsymbol{\Sigma}_t$	$\frac{\sigma_x^2 \sigma_t^2}{\sigma_x^2 + \sigma_t^2} \mathbf{I}$	$\lambda^2 (1 - e^{-2\bar{\theta}_t t}) \mathbf{I}$	$\frac{\sigma_{t,1}^2 \sigma_{t,1}^2}{\sigma_{t,1}^2} \mathbf{I}$	$\sigma_t^2 (1 - \frac{\text{SNR}_t}{\text{SNR}_t}) \mathbf{I}$	$\gamma_t \mathbf{A}^+ \boldsymbol{\Sigma} \mathbf{A}^{+\top} + \beta_t (\mathbf{I} - \mathbf{A}^+ \mathbf{A})$
Markovian	$\times$	$\times$	$\times$	$\times$	$\checkmark$
Hyperparameters	$\beta_t = \int_0^t g^2(\tau) d\tau, \sigma_t^2 = \int_0^t g^2(\tau) d\tau$	$\theta_t = \frac{\sigma_t^2}{\lambda^2}, \bar{\theta}_t = \int_s^t \theta_\tau d\tau, \bar{\sigma}_{s,t}^2 = \frac{g^2(t)}{2\theta_t} (1 - e^{-2\bar{\theta}_t s t})$	$\theta_t = \frac{g^2(t)}{2\lambda^2}, \bar{\theta}_t = \int_s^t \theta_\tau d\tau, \bar{\sigma}_{s,t}^2 = \frac{g^2(t)}{2\theta_t} (1 - e^{-2\bar{\theta}_t s t})$	$\text{SNR}_t = \frac{\alpha_t^2}{\sigma_t^2}, \alpha_t = \exp\left(-\frac{1}{2} \int_0^t g^2(\tau) d\tau\right), \sigma_t^2 = 1 - \alpha_t^2$	$\alpha_t, \beta_t, \gamma_t$ follow from theorem 2

## 5 Experiments

**Baselines.** We compare SDB with both supervised bridge methods and unsupervised plug-and-play diffusion-based baselines. For the former, we include I2SB [Liu et al., 2023], IR-SDE [Luo et al., 2023a], GOUB [Yue et al., 2024], and DDBM [Zhou et al., 2024]. For the latter, we pick DPS [Chung et al., 2023a], IIGDM [Song et al., 2023a], and DDNM [Wang et al., 2023], all of which rely on the assumption of a noisy linear measurement model. Detailed descriptions of all baselines are provided in the Appendix. Unlike these methods, which rely on scalar SDEs, SDB introduces a more general matrix-valued formulation that allows structured control over range and null space components. We summarize the resulting conceptual differences to baseline bridge methods in table 1. Following standard evaluation practice [Luo et al., 2023a, Yue et al., 2024], we report perceptual scores (FID [Heusel et al., 2017], LPIPS [Zhang et al., 2018]) and reconstruction metrics (PSNR, SSIM).

**Experimental design.** To isolate the contribution of SDB as a diffusion process, we standardize key implementation details across all methods. Specifically: (i) for both supervised and unsupervised approaches, we train score networks from scratch using the training hyperparameters and architecture of Luo et al. [2023a], with 256 training epochs for supervised methods and 512 for unsupervised

Table 2: Quantitative comparison of SDB with the baselines across four inverse problems. **Bold** indicates best and underline second-best values for each metric.

Method	Inpainting - CelebA-HQ				Superresolution - DIV2K				CT Reconstruction - RSNA				MRI Reconstruction - Br35H			
	FID ↓	LPIPS ↓	PSNR ↑	SSIM ↑	FID ↓	LPIPS ↓	PSNR ↑	SSIM ↑	FID ↓	LPIPS ↓	PSNR ↑	SSIM ↑	FID ↓	LPIPS ↓	PSNR ↑	SSIM ↑
<b>Unsupervised</b>																
DPS	12.3	0.213	18.59	0.684	101.2	0.295	19.04	0.492	29.251	0.160	32.870	0.709	40.73	0.187	21.336	0.549
IIGDM	10.2	0.146	19.02	0.762	97.09	0.311	18.84	0.530	32.287	0.165	31.272	0.757	41.14	0.211	19.830	0.665
DDNM	10.7	0.112	18.90	0.791	99.21	0.302	17.13	0.513	30.411	0.238	27.226	0.783	42.23	0.196	18.122	0.636
<b>Supervised</b>																
I2SB	5.56	0.047	27.41	0.889	<u>83.73</u>	<b>0.176</b>	25.21	0.686	24.812	0.107	41.886	0.924	31.54	0.065	28.750	0.849
IR-SDE	4.68	0.031	29.92	0.912	96.22	0.185	23.51	0.603	18.884	0.028	43.438	0.964	30.14	0.065	28.878	0.871
GOUB	4.69	<u>0.031</u>	29.89	0.912	98.89	<u>0.178</u>	24.39	0.649	19.899	0.024	43.878	0.967	<u>30.63</u>	<u>0.058</u>	28.590	0.863
DDBM	6.03	0.047	28.15	0.906	90.16	0.233	25.79	<u>0.720</u>	23.357	0.040	44.415	0.964	32.42	0.074	28.971	0.872
<b>Ours</b>																
SDB (VP)	4.90	<b>0.030</b>	<u>30.51</u>	0.914	87.08	0.228	<u>25.91</u>	<b>0.724</b>	15.425	0.019	<u>46.365</u>	<u>0.981</u>	32.88	0.068	<u>29.255</u>	<u>0.881</u>
SDB (VE)	5.97	0.042	<b>32.12</b>	<b>0.944</b>	94.73	0.226	25.90	0.718	<b>14.168</b>	0.020	46.325	<u>0.981</u>	33.90	0.083	29.098	0.876
SDB (SB)	<b>4.63</b>	<u>0.031</u>	30.40	<u>0.930</u>	<b>81.56</b>	0.226	<b>26.10</b>	<b>0.724</b>	<u>15.016</u>	<b>0.018</b>	<b>46.672</b>	<b>0.982</b>	<b>29.85</b>	<b>0.053</b>	<b>29.812</b>	<b>0.893</b>

ones; (ii) each supervised method learns a mapping between signal samples and their PRs, ensuring that SDB does not benefit from a favorable parameterization, particularly in settings where  $m \neq d$ ; (iii) during evaluation, supervised methods use 100 discretization steps, while unsupervised methods use 200, along with a standard Euler–Maruyama solver and their optimal noise schedule (e.g., VP for DDBM). To ensure consistent evaluation, we reimplement all methods within a unified framework, allowing for the separation of algorithmic advancements from the proposed stochastic process.

**Benchmarks.** We evaluate SDB on four inverse problems with varying measurement system complexities, using original images at a resolution of  $256 \times 256$ . Building on prior work [Luo et al., 2023a, Yue et al., 2024], we first consider **inpainting on CelebA-HQ** [Karras et al., 2018], where  $\mathbf{A}$  is a masking operator and  $\Sigma = \mathbf{0}_{m \times m}$  (noiseless). The measurements consist of the masked original images ( $m = d$ ), which are equivalent to the PRs ( $\mathbf{A}^+ = \mathbf{I}$ ). Additionally, we follow previous studies by examining **superresolution on DIV2K** [Agustsson and Timofte, 2017, Timofte et al., 2017], where  $\mathbf{A}$  represents a  $4 \times$  downsampling operator ( $d = 4m$ ), implemented through average pooling. For this task,  $\mathbf{A}^+$  reconstructs the images using nearest-neighbor interpolation. To evaluate more complex and practical inverse problems, we additionally propose two medical imaging tasks: **CT reconstruction on the RSNA Intracranial Hemorrhage dataset** [Anouk Stein et al., 2019] and **MRI reconstruction on the Br35H dataset** [Merlin, 2022], both using 2D axial brain scan slices.

For CT reconstruction, the sinogram  $\mathbf{y}$  represents line integrals of the object’s attenuation coefficient, with the system matrix  $\mathbf{A}$  describing detector-specific integrations along X-ray trajectories. We implement  $\mathbf{A}$  using its SVD decomposition,  $\mathbf{A} = \mathbf{U}\mathbf{D}\mathbf{V}^*$ . To make the problem more realistic and introduce domain-specific artifacts, we zero the singular values of  $\mathbf{D}$  below a threshold  $\tau = 3.2$  and use a noisy setting with scalar covariance  $\Sigma = \sigma_1^2 \mathbf{I}$ , where  $\sigma_1^2 = 0.0001$ .

For MRI reconstruction,  $\mathbf{y}$  consists of undersampled Fourier-domain measurements. The system matrix is modeled as  $\mathbf{A} = \mathbf{M}\mathcal{F}$ , where  $\mathcal{F}$  is the Fourier transform and  $\mathbf{M}$  is a masking matrix. We sample  $\mathbf{M}$  such that  $\lambda_1$  controls the percentage of the lowest frequencies to be kept (a deterministic operation), while  $\lambda_2$  specifies the percentage of frequencies to sample from the remaining ones (a stochastic operation). The noisy setting is similarly modeled with a scalar covariance matrix  $\Sigma = \sigma_2^2 \mathbf{I}$ , where  $\sigma_2^2 = 5.0$ . We pick  $\lambda_1 = 16$  and  $\lambda_2 = 30$  as defaults.

## 5.1 General evaluation

The results summarized in table 2 show that SDB (SB) outperforms all baseline methods across every metric, with the exception of LPIPS on DIV2K. Notably, SDB (SB) demonstrates a clear advantage over I2SB, which shares the most similar stochastic process, highlighting how SDB (SB) effectively leverages additional information from the measurement system. Overall, it also provides empirical justification for the null space OT plan mentioned in theorem 2. Moreover, SDB (SB) displays superior stability, as the performance rankings of the baseline bridge methods exhibit more variability across tasks.

SDB (VE) and SDB (VP) strike a different balance between perceptual and reconstruction metrics compared to SDB (SB). In inpainting, they often outperform all other methods, with a noticeable emphasis on reconstruction quality. This trend is even more pronounced in the superresolution and MRI reconstruction tasks. In CT reconstruction, their performance is nearly on par with SDB (SB).

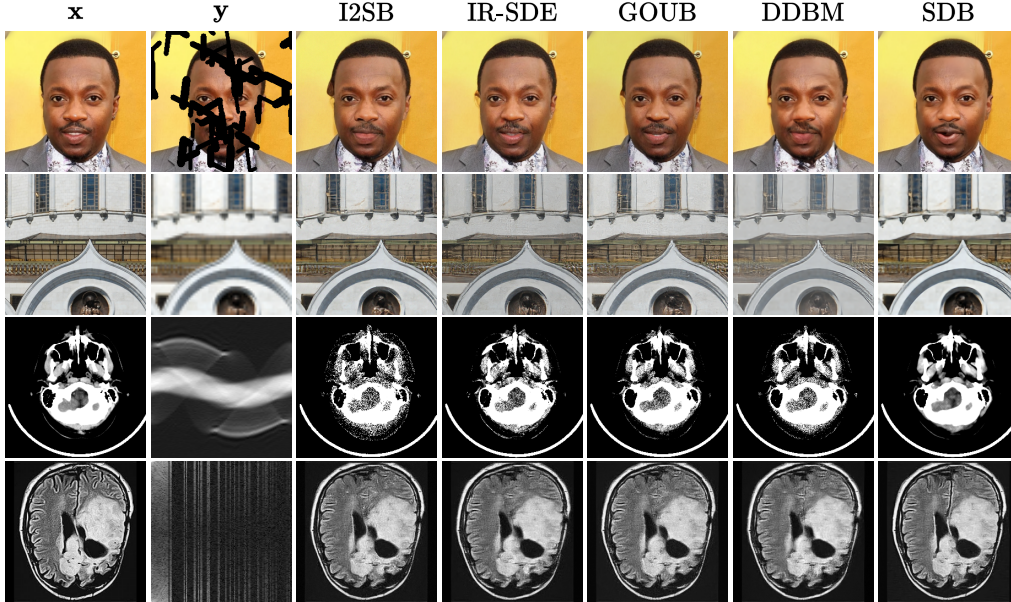


Figure 2: Qualitative comparison of SDB (SB) with the best-performing baselines (bridge methods). Rows depict the results for inpainting, superresolution, CT and MRI reconstruction respectively.

Although they occasionally underperform relative to baseline bridge methods, this is not unexpected given the nature of their stochastic process. Along with IR-SDE, these methods are unique in not treating  $p(x_1)$  as a sum of Dirac deltas, which means they start the reverse process from a noisy sample. This additional noise may make the problem more challenging, but when directly comparing SDB (VE) and SDB (VP) to IR-SDE, the performance improvements become evident.

Finally, under our unified setting, prior bridge methods demonstrate comparable performance with significantly reduced variability compared to what previous works report [Luo et al., 2023a, Yue et al., 2024]. For instance, their PSNR on the MRI reconstruction task falls within the range of  $[28.590, 28.971]$ , meaning that performance gains on the order of  $\approx 0.2$  can be considered significant in this context. Notably, the unsupervised baselines exhibit visibly lower performance compared to bridge methods. While this is expected due to the lack of training with paired data, we note that our setup allocates only twice the training budget to the unconditional models compared to the bridge methods, suggesting that their performance has not yet saturated. We consider improving these models as future work.

## 5.2 Evaluation under a misspecified model

In practice, while the general form of the measurement system in an inverse problem may be known, the specific parameter values often differ between training and deployment. This creates a generalization challenge, where the model must learn the underlying dynamics rather than relying on shortcuts. For example, in CT reconstruction, a well-trained model should perform stably near the original parameter  $\tau$ . A larger  $\tau'$ , which reduces low-frequency information, makes the task more difficult. However, a generalized model should maintain most of its performance as long as  $\tau'$  remains reasonably close to  $\tau$ .

This issue is particularly critical for SDB, where the measurement system’s parameters are embedded directly into the coefficients of its stochastic process. While results in section 5.1 indicate performance gains, deploying SDB in practice could be risky if it overfits to specific parameter values. Therefore, the following experiment tests whether SDB can generalize when evaluated under a misspecified model. For this evaluation, we focus on the best-performing methods from section 5.1, namely the baseline bridge methods and the SB variant of SDB.

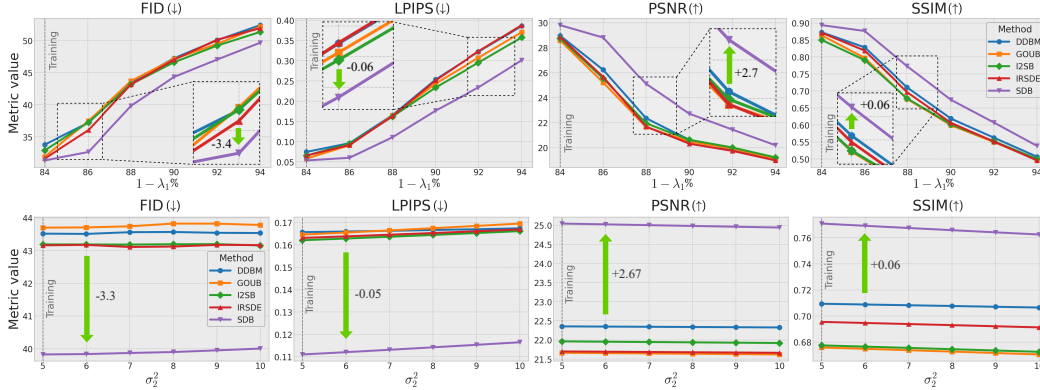


Figure 3: Quantitative comparison of SDB (SB) with other bridge methods in a misspecified MRI reconstruction setting. The **top** row evaluates bridges trained with  $\lambda_1 = 16$ ,  $\sigma_2^2 = 5$  on data generated from systems with decreasing  $\lambda_1$ . The **bottom** row evaluates performance on data with  $\lambda_1 = 14$  and increasing  $\sigma_2^2$ . Perturbing the original system makes the problem harder in both cases.

**Improved generalization.** We begin with the MRI reconstruction task, where the system response matrix preserves a portion of the original signal by keeping  $\lambda_1$  of the frequencies, starting from the lowest. This maintains the general structure of the true image, and as  $\lambda_1$  is gradually decreased, more information is lost, making the task increasingly difficult. This scenario also mirrors real-world situations where a detector captures fewer measurements.

In what follows, we evaluate the checkpoints of bridge methods trained under a default setting ( $\lambda_1 = 16$ ,  $\lambda_2 = 30$ ,  $\sigma_2^2 = 5.0$ ) on measurements generated from a system with modified parameters. Figure 3 (top) shows the performance of the methods as  $\lambda_1$  is gradually decreased. Notably, the performance gap between SDB and the baseline methods widens as early as  $\lambda_1 = 14$ , and this advantage is sustained even at lower values. SDB continues to better utilize the available measurement information, indicating much greater robustness to reductions in  $\lambda_1$ .

To make the setting even more challenging, we set  $\lambda_1 = 14$  and gradually increase the measurement noise variance  $\sigma_2^2$  to up to twice its training-time value, simulating a more realistic scenario. Figure 3 (bottom) shows that, even under this perturbation, SDB maintains a significant performance advantage over the baseline methods. Unsurprisingly, all methods exhibit greater robustness to changes in  $\sigma_2^2$ , which is expected due to their denoising nature.

An analogous analysis for the CT reconstruction task is provided in the Appendix, yielding similar observations. Both experiments, closely aligned with the practical applications of inverse problem solvers, underscore the generalization capabilities of SDB across a broad range of system perturbations, positioning it as a promising solution for real-world scenarios.

**Extended evaluation.** In addition to CT reconstruction in a misspecified setting, we provide a broader evaluation of all SDB variants, ablation studies and qualitative results in the Appendix.

## 6 Discussion and limitations

SDB offers a principled framework for constructing measurement-system-specific diffusion bridges tailored to inverse problems under a linear Gaussian model. By explicitly incorporating information about the measurement system into the generative process, it achieves improved reconstruction quality and exhibits strong generalization under system perturbations. However, the method also comes with natural limitations. Notably, extending SDB to nonlinear measurement systems remains an open challenge. While local linearization may offer a potential workaround, it relies on differentiability and has yet to be validated in practice. In addition, our work adopts simple variance schedules for both the range and null space components; the interplay between these two processes warrants further theoretical and empirical investigation to identify optimal scheduling strategies. From a real-world application perspective, tasks such as CT and MRI reconstruction are typically performed in three dimensions—evaluating our method in such settings remains an open direction for future work. Despite these limitations, we view SDB as a valuable contribution to the growing literature on diffusion-based inverse problem solvers and a promising foundation for future research.

## References

- B. P. Abbott et al. Observation of gravitational waves from a binary black hole merger. In *Physical Review Letters*. American Physical Society, 2016.
- Eirikur Agustsson and Radu Timofte. Ntire 2017 challenge on single image super-resolution: Dataset and study. In *The IEEE Conference on Computer Vision and Pattern Recognition (CVPR) Workshops*, July 2017.
- Kazunori Akiyama et al. First M87 event horizon telescope results. i. the shadow of the supermassive black hole. In *Proceedings of the Event Horizon Telescope Imaging*, 2019.
- Brian DO Anderson. *Reverse-time diffusion equation models*, volume 12. Stochastic Processes and their Applications, Elsevier, 1982.
- MD Anouk Stein, Carol Wu, Chris Carr, George Shih, Jayashree Kalpathy-Cramer, Julia Elliott, kalpathy, Luciano Prevedello, MD Marc Kohli, Matt Lungren, Phil Culliton, Robyn Ball, and Safwan Halabi MD. Rsnai intracranial hemorrhage detection. <https://kaggle.com/competitions/rsnai-intracranial-hemorrhage-detection>, 2019. Kaggle.
- Georgios Batzolis, Jan Stanczuk, Carola-Bibiane Schönlieb, and Christian Etmann. Conditional image generation with score-based diffusion models. In *arXiv preprint arXiv:2111.13606*, 2021.
- M Bertero, C De Mol, and E R Pike. Linear inverse problems with discrete data. i. general formulation and singular system analysis. In *Inverse Problems*, 1985.
- E.J. Candes, J. Romberg, and T. Tao. Robust uncertainty principles: exact signal reconstruction from highly incomplete frequency information. In *IEEE Transactions on Information Theory*, 2006.
- Liangyu Chen, Xiaojie Chu, Xiangyu Zhang, and Jian Sun. Simple baselines for image restoration. In *European conference on computer vision*, 2022.
- Hyungjin Chung, Byeongsu Sim, Dohoon Ryu, and Jong Chul Ye. Improving diffusion models for inverse problems using manifold constraints. In *Advances in Neural Information Processing Systems*, 2022.
- Hyungjin Chung, Jeongsol Kim, Michael Thompson Mccann, Marc Louis Klasky, and Jong Chul Ye. Diffusion posterior sampling for general noisy inverse problems. In *The Eleventh International Conference on Learning Representations*, 2023a.
- Hyungjin Chung, Jeongsol Kim, and Jong Chul Ye. Direct diffusion bridge using data consistency for inverse problems. In *Advances in Neural Information Processing Systems*, 2023b.
- Hyungjin Chung, Suhyeon Lee, and Jong Chul Ye. Decomposed diffusion sampler for accelerating large-scale inverse problems. In *The Twelfth International Conference on Learning Representations*, 2024.
- Antonia Creswell and Anil Anthony Bharath. Inverting the generator of a generative adversarial network. In *IEEE transactions on neural networks and learning systems*, 2018.
- Giannis Daras, Hyungjin Chung, Chieh-Hsin Lai, Yuki Mitsufuji, Jong Chul Ye, Peyman Milanfar, Alexandros G Dimakis, and Mauricio Delbracio. A survey on diffusion models for inverse problems. In *arXiv preprint arXiv:2410.00083*, 2024.
- Valentin De Bortoli, James Thornton, Jeremy Heng, and Arnaud Doucet. Diffusion schrödinger bridge with applications to score-based generative modeling. *Advances in Neural Information Processing Systems*, 2021.
- Mauricio Delbracio and Peyman Milanfar. Inversion by direct iteration: An alternative to denoising diffusion for image restoration. In *Transactions on Machine Learning Research*, 2023.
- Prafulla Dhariwal and Alex Nichol. Diffusion models beat gans on image synthesis. In *Advances in neural information processing systems*, 2021.

- Joseph L Doob. *Classical potential theory and its probabilistic counterpart*, volume 262. Springer, 1984.
- Tomer Garber and Tom Tirer. Image restoration by denoising diffusion models with iteratively preconditioned guidance. In *Proceedings of the IEEE/CVF Conference on Computer Vision and Pattern Recognition (CVPR)*, 2024.
- Daniel T Gillespie. Exact numerical simulation of the ornstein-uhlenbeck process and its integral. *Physical review E*, 1996.
- Guande He, Kaiwen Zheng, Jianfei Chen, Fan Bao, and Jun Zhu. Consistency diffusion bridge models. In *Advances in Neural Information Processing Systems*, 2024.
- Jeremy Heng, Valentin De Bortoli, Arnaud Doucet, and James Thornton. Simulating diffusion bridges with score matching. In *arXiv preprint arXiv:2111.07243*, 2021.
- Martin Heusel, Hubert Ramsauer, Thomas Unterthiner, Bernhard Nessler, and Sepp Hochreiter. Gans trained by a two time-scale update rule converge to a local nash equilibrium. In *Advances in neural information processing systems*, 2017.
- Jonathan Ho, Ajay Jain, and Pieter Abbeel. Denoising diffusion probabilistic models. In *Advances in neural information processing systems*, 2020.
- Tero Karras, Timo Aila, Samuli Laine, and Jaakko Lehtinen. Progressive growing of gans for improved quality, stability, and variation. In *International Conference on Learning Representations*, 2018.
- Bahjat Kawar, Michael Elad, Stefano Ermon, and Jiaming Song. Denoising diffusion restoration models. In *Advances in Neural Information Processing Systems*, 2022.
- Diederik P. Kingma and Jimmy Ba. Adam: A method for stochastic optimization. In *International Conference on Learning Representations*, 2015.
- Guan-Hong Liu, Arash Vahdat, De-An Huang, Evangelos Theodorou, Weili Nie, and Anima Anandkumar. I2SB: Image-to-Image Schrödinger Bridge. In *International Conference on Machine Learning*, 2023.
- Xingchao Liu, Lemeng Wu, Mao Ye, and qiang liu. Let us build bridges: Understanding and extending diffusion generative models. In *NeurIPS 2022 Workshop on Score-Based Methods*, 2022.
- Ziwei Luo, Fredrik K Gustafsson, Zheng Zhao, Jens Sjölund, and Thomas B Schön. Image restoration with mean-reverting stochastic differential equations. In *International Conference on Machine Learning*, 2023a.
- Ziwei Luo, Fredrik K Gustafsson, Zheng Zhao, Jens Sjölund, and Thomas B Schön. Refusion: Enabling large-size realistic image restoration with latent-space diffusion models. In *Proceedings of the IEEE/CVF conference on computer vision and pattern recognition*, pages 1680–1691, 2023b.
- Morteza Mardani, Jiaming Song, Jan Kautz, and Arash Vahdat. A variational perspective on solving inverse problems with diffusion models. In *The Twelfth International Conference on Learning Representations*, 2024.
- Merlin. Br35h : 2020. <https://www.heywhale.com/mw/dataset/61d3e5682d30dc001701f728>, 2022.
- Toshio Mikami. Monge’s problem with a quadratic cost by the zero-noise limit of h-path processes. In *Probability theory and related fields*, 2004.
- Jennifer L Mueller and Samuli Siltanen. *Linear and nonlinear inverse problems with practical applications*. SIAM, 2012.
- Gregory Ongie, Ajil Jalal, Christopher A. Metzler, Richard G. Baraniuk, Alexandros G. Dimakis, and Rebecca Willett. Deep learning techniques for inverse problems in imaging. In *IEEE Journal on Selected Areas in Information Theory*, 2020.

- Stefano Peluchetti. Non-denoising forward-time diffusions, 2022. URL <https://openreview.net/forum?id=oVfIKuhqfC>.
- Julius Richter, Simon Welker, Jean-Marie Lemerrier, Bunlong Lay, and Timo Gerkmann. Speech enhancement and dereverberation with diffusion-based generative models. In *IEEE/ACM Transactions on Audio, Speech, and Language Processing*, 2023.
- Herbert E Robbins. An empirical Bayes approach to statistics. In *Breakthroughs in Statistics: Foundations and basic theory*, 1992.
- Simo Särkkä and Arno Solin. *Applied stochastic differential equations*, volume 10. Cambridge University Press, 2019.
- Erwin Schrödinger. Sur la théorie relativiste de l'électron et l'interprétation de la mécanique quantique. In *Annales de l'institut Henri Poincaré*, volume 2, pages 269–310, 1932.
- Yuyang Shi, Valentin De Bortoli, Andrew Campbell, and Arnaud Doucet. Diffusion schrödinger bridge matching. *Advances in Neural Information Processing Systems*, 2024.
- Jascha Sohl-Dickstein, Eric Weiss, Niru Maheswaranathan, and Surya Ganguli. Deep unsupervised learning using nonequilibrium thermodynamics. In *International Conference on Machine Learning*, 2015.
- Vignesh Ram Somnath, Matteo Pariset, Ya-Ping Hsieh, Maria Rodriguez Martinez, Andreas Krause, and Charlotte Bunne. Aligned diffusion schrödinger bridges. In *Uncertainty in Artificial Intelligence*. PMLR, 2023.
- Jiaming Song, Chenlin Meng, and Stefano Ermon. Denoising diffusion implicit models. In *International Conference on Learning Representations*, 2021a.
- Jiaming Song, Arash Vahdat, Morteza Mardani, and Jan Kautz. Pseudoinverse-guided diffusion models for inverse problems. In *International Conference on Learning Representations*, 2023a.
- Yang Song and Stefano Ermon. Generative modeling by estimating gradients of the data distribution. In *Advances in neural information processing systems*, 2019.
- Yang Song, Jascha Sohl-Dickstein, Diederik P Kingma, Abhishek Kumar, Stefano Ermon, and Ben Poole. Score-based generative modeling through stochastic differential equations. In *International Conference on Learning Representations*, 2021b.
- Yang Song, Prafulla Dhariwal, Mark Chen, and Ilya Sutskever. Consistency models. In *International Conference on Machine Learning*, 2023b.
- Gilbert Strang. *Introduction to linear algebra*. SIAM, 2022.
- Albert Tarantola. *Inverse problem theory and methods for model parameter estimation*. SIAM, 2005.
- Radu Timofte, Eirikur Agustsson, Luc Van Gool, Ming-Hsuan Yang, Lei Zhang, Bee Lim, et al. Ntire 2017 challenge on single image super-resolution: Methods and results. In *The IEEE Conference on Computer Vision and Pattern Recognition (CVPR) Workshops*, 2017.
- Matthew Tivnan, Jacopo Teneggi, Tzu-Cheng Lee, Ruoqiao Zhang, Kirsten Boedeker, Liang Cai, Grace J. Gang, Jeremias Sulam, and J. Webster Stayman. Fourier diffusion models: A method to control mtf and nps in score-based stochastic image generation. In *IEEE Transactions on Medical Imaging*, 2025.
- Yinhui Wang, Jiwen Yu, and Jian Zhang. Zero-shot image restoration using denoising diffusion null-space model. In *International Conference on Learning Representations*, 2023.
- Simon Welker, Julius Richter, and Timo Gerkmann. Speech enhancement with score-based generative models in the complex stft domain. In *Interspeech*, 2022.
- Conghan Yue, Zhengwei Peng, Junlong Ma, Shiyan Du, Pengxu Wei, and Dongyu Zhang. Image restoration through generalized ornstein-uhlenbeck bridge. In *International Conference on Machine Learning*, 2024.

- Richard Zhang, Phillip Isola, Alexei A Efros, Eli Shechtman, and Oliver Wang. The unreasonable effectiveness of deep features as a perceptual metric. In *Proceedings of the IEEE conference on computer vision and pattern recognition*, 2018.
- Kaiwen Zheng, Guande He, Jianfei Chen, Fan Bao, and Jun Zhu. Diffusion bridge implicit models. In *The Thirteenth International Conference on Learning Representations*, 2025.
- Linqi Zhou, Aaron Lou, Samar Khanna, and Stefano Ermon. Denoising diffusion bridge models. In *International Conference on Learning Representations*, 2024.
- Kaizhen Zhu, Mokai Pan, Yuexin Ma, Yanwei Fu, Jingyi Yu, Jingya Wang, and Ye Shi. Unidb: A unified diffusion bridge framework via stochastic optimal control. In *arXiv preprint arXiv:2502.05749*, 2025.

## Appendix for "System-Embedded Diffusion Bridge Models"

<b>A Proofs and derivations</b>	<b>14</b>
A.1 Derivation of drift and diffusion coefficients for SDB . . . . .	14
A.2 Proof of theorem 2 . . . . .	15
<b>B Extended related works</b>	<b>16</b>
B.1 Diffusion models for inverse problems . . . . .	16
B.2 Diffusion and Schrödinger bridges. . . . .	17
B.3 Baselines . . . . .	17
<b>C Extended methodology</b>	<b>19</b>
C.1 Network parameterization . . . . .	19
C.2 Nonlinear measurement systems . . . . .	19
C.3 Pseudocode . . . . .	19
<b>D Experimental setup</b>	<b>19</b>
D.1 Training hyperparameters . . . . .	19
D.2 Computational requirements . . . . .	19
<b>E Additional experimental results</b>	<b>20</b>
E.1 Evaluation under a misspecified model (CT reconstruction) . . . . .	20
E.2 Hyperparameter analysis . . . . .	20
<b>F Broader impact</b>	<b>22</b>
<b>G Additional visual results</b>	<b>22</b>

### A Proofs and derivations

#### A.1 Derivation of drift and diffusion coefficients for SDB

We begin with deriving the drift and diffusion coefficients  $\mathbf{F}_t, \mathbf{G}_t$  of SDB (eqs. (10a) and (10b)) by using theorem 1 with the mean and covariance matrices  $\mathbf{H}_t, \Sigma_t$  (eqs. (8a) and (8b)) of its forward process. Recall that  $\mathbf{H}_t = \mathbf{A}^+ \mathbf{A} + \alpha_t (\mathbf{I} - \mathbf{A}^+ \mathbf{A}), \Sigma_t = \gamma_t \mathbf{A}^+ \Sigma \mathbf{A}^{+\top} + \beta_t (\mathbf{I} - \mathbf{A}^+ \mathbf{A})$ . Following theorem 1, we obtain

$$\mathbf{A}^+ \mathbf{A} \mathbf{F}_t = \frac{d}{dt} \mathbf{A}^+ \mathbf{A} \log \mathbf{H}_t = \frac{d}{dt} \mathbf{A}^+ \mathbf{A} = \mathbf{0}, \quad (12a)$$

$$(\mathbf{I} - \mathbf{A}^+ \mathbf{A}) \mathbf{F}_t = \frac{d}{dt} \log \alpha_t (\mathbf{I} - \mathbf{A}^+ \mathbf{A}), \quad (12b)$$

$$\frac{d}{dt} \mathbf{A}^+ \mathbf{A} \Sigma_t = \frac{d\gamma_t}{dt} \mathbf{A}^+ \Sigma \mathbf{A}^{+\top}, \quad (12c)$$

$$\frac{d}{dt} (\mathbf{I} - \mathbf{A}^+ \mathbf{A}) \Sigma_t = \frac{d\beta_t}{dt} (\mathbf{I} - \mathbf{A}^+ \mathbf{A}). \quad (12d)$$

Moreover, note that  $\mathbf{F}_t^\top = \mathbf{F}_t, \Sigma_t^\top = \Sigma_t$  due to the symmetry of the range and null space projections, and  $\mathbf{F}_t \Sigma_t = \Sigma_t \mathbf{F}_t$  since  $\mathbf{F}_t$  only affects the null space and  $(\mathbf{I} - \mathbf{A}^+ \mathbf{A})^2 = (\mathbf{I} - \mathbf{A}^+ \mathbf{A})$  (idempotent).

Following theorem 1,

$$\mathbf{F}_t = \frac{d}{dt} \log \alpha_t (\mathbf{I} - \mathbf{A}^+ \mathbf{A}), \quad (13a)$$

$$\mathbf{G}_t \mathbf{G}_t = \frac{d\boldsymbol{\Sigma}_t}{dt} - \mathbf{F}_t \boldsymbol{\Sigma}_t - \boldsymbol{\Sigma}_t \mathbf{F}_t^\top \quad (13b)$$

$$= \frac{d\boldsymbol{\Sigma}_t}{dt} - 2\mathbf{F}_t \boldsymbol{\Sigma}_t \quad (13c)$$

$$= \frac{d\gamma_t}{dt} \mathbf{A}^+ \boldsymbol{\Sigma} \mathbf{A}^{+\top} + \left( \frac{d\beta_t}{dt} - 2\beta_t \frac{d}{dt} \log \alpha_t \right) (\mathbf{I} - \mathbf{A}^+ \mathbf{A}). \quad (13d)$$

## A.2 Proof of theorem 2

We begin by recalling two propositions of Liu et al. [2023] using our notation, which will serve as the basis of the proof.

**Proposition 1 (Analytic posterior given boundary pair) [Liu et al., 2023]** *The posterior of eq. (1) given some boundary pair  $(\mathbf{x}_0, \mathbf{x}_1)$  admits an analytic form:*

$$p(\mathbf{x}_t | \mathbf{x}_0, \mathbf{x}_1) = \mathcal{N}(\boldsymbol{\mu}_t(\mathbf{x}_0, \mathbf{x}_1), \boldsymbol{\Sigma}_t), \quad (14)$$

where  $\boldsymbol{\mu}_t = \frac{\bar{\sigma}_t^2}{\bar{\sigma}_t^2 + \sigma_t^2} \mathbf{x}_0 + \frac{\sigma_t^2}{\bar{\sigma}_t^2 + \sigma_t^2} \mathbf{x}_1$ ,  $\boldsymbol{\Sigma}_t = \frac{\sigma_t^2 \bar{\sigma}_t^2}{\bar{\sigma}_t^2 + \sigma_t^2} \mathbf{I}$  and  $\sigma_t^2 = \int_0^t g^2(\tau) d\tau$ ,  $\bar{\sigma}_t^2 = \int_t^1 g^2(\tau) d\tau$  with  $\mathbf{G}_t = g(t)\mathbf{I}$ .

**Proposition 2 (Optimal Transport ODE; OT-ODE) [Liu et al., 2023]** *When  $g^2(t) \rightarrow 0$ , the SDE between  $(\mathbf{x}_0, \mathbf{x}_1)$  reduces to an ODE:*

$$d\mathbf{x}_t = \mathbf{v}_t(\mathbf{x}_t | \mathbf{x}_0) dt, \quad (15)$$

where  $\mathbf{v}_t(\mathbf{x}_t | \mathbf{x}_0) = \frac{g^2(t)}{\sigma_t^2} (\mathbf{x}_t - \mathbf{x}_0)$  whose solution is the posterior mean of eq. (14).

Consider the null space part of  $\mathbf{x}_t$  given by mean and covariance matrices from eqs. (8a) and (8b) with  $\alpha_t = \frac{\bar{\sigma}_t^2}{\bar{\sigma}_t^2 + \sigma_t^2}$ ,  $\beta_t = \frac{\sigma_t^2}{\bar{\sigma}_t^2 + \sigma_t^2}$  for  $\sigma_t^2 = \int_0^t g^2(\tau) d\tau$ ,  $\bar{\sigma}_t^2 = \int_t^1 g^2(\tau) d\tau$ , where  $g(t)$  is the null space diffusion coefficient given by eq. (10b), i.e.,  $g(t) = \left( \frac{d\beta_t}{dt} - 2\beta_t \frac{d}{dt} \log \alpha_t \right)^{\frac{1}{2}}$ :

$$(\mathbf{I} - \mathbf{A}^+ \mathbf{A}) \mathbf{x}_t = \frac{\bar{\sigma}_t^2}{\bar{\sigma}_t^2 + \sigma_t^2} (\mathbf{I} - \mathbf{A}^+ \mathbf{A}) \mathbf{x}_0 + \left( \frac{\sigma_t^2 \bar{\sigma}_t^2}{\bar{\sigma}_t^2 + \sigma_t^2} \right)^{\frac{1}{2}} (\mathbf{I} - \mathbf{A}^+ \mathbf{A}) \boldsymbol{\epsilon} \quad (16)$$

for  $\boldsymbol{\epsilon} \sim \mathcal{N}(\mathbf{0}_d, \mathbf{I}_{d \times d})$ . Note that the null space part of  $\mathbf{x}_1$ , being the PR of  $\mathbf{x}_0$ , is zeroed out, i.e.,  $(\mathbf{I} - \mathbf{A}^+ \mathbf{A}) \mathbf{x}_1 = (\mathbf{I} - \mathbf{A}^+ \mathbf{A}) \mathbf{0}_{d \times d}$ . This allows us to artificially rewrite  $\mathbf{x}_t$  as

$$(\mathbf{I} - \mathbf{A}^+ \mathbf{A}) \mathbf{x}_t = (\mathbf{I} - \mathbf{A}^+ \mathbf{A}) \left( \frac{\bar{\sigma}_t^2}{\bar{\sigma}_t^2 + \sigma_t^2} \mathbf{x}_0 + \frac{\sigma_t^2}{\bar{\sigma}_t^2 + \sigma_t^2} \mathbf{0}_{d \times d} \right) + \left( \frac{\sigma_t^2 \bar{\sigma}_t^2}{\bar{\sigma}_t^2 + \sigma_t^2} \right)^{\frac{1}{2}} (\mathbf{I} - \mathbf{A}^+ \mathbf{A}) \boldsymbol{\epsilon}. \quad (17)$$

Equivalently,  $(\mathbf{I} - \mathbf{A}^+ \mathbf{A}) \mathbf{x}_t \sim \mathcal{N}((\mathbf{I} - \mathbf{A}^+ \mathbf{A}) \left( \frac{\bar{\sigma}_t^2}{\bar{\sigma}_t^2 + \sigma_t^2} \mathbf{x}_0 + \frac{\sigma_t^2}{\bar{\sigma}_t^2 + \sigma_t^2} \mathbf{x}_1 \right), \frac{\sigma_t^2 \bar{\sigma}_t^2}{\bar{\sigma}_t^2 + \sigma_t^2} (\mathbf{I} - \mathbf{A}^+ \mathbf{A}))$ . Hence, the posterior mean of SDB (SB) takes the form stated in proposition 1 and proposition 2 can be applied directly to the null space part.

As a final remark, we note that, up to this point, the definition of  $g(t)$  is interdependent with that of  $\alpha_t$  and  $\beta_t$ . It is not immediately clear that defining  $\alpha_t, \beta_t$  as in theorem 2 fulfills  $g^2(t) = \frac{d\beta_t}{dt} - 2\beta_t \frac{d}{dt} \log \alpha_t$ . We now show that this property is indeed satisfied.

Denote by  $C = \sigma_t^2 + \bar{\sigma}_t^2$  and observe that  $\beta_t = \sigma_t^2 \alpha_t$ ,  $\bar{\sigma}_t^2 = C - \sigma_t^2$ ,  $\frac{d\sigma_t^2}{dt} = g^2(t)$ . Then,

$$\frac{d}{dt} \log \alpha_t = \frac{d}{dt} \log \frac{\bar{\sigma}_t^2}{\bar{\sigma}_t^2 + \sigma_t^2} \quad (18a)$$

$$= \frac{d}{dt} (\log \bar{\sigma}_t^2 - \log C) \quad (18b)$$

$$= \frac{g^2(t)}{\bar{\sigma}_t^2}, \quad (18c)$$

$$\frac{d\beta_t}{dt} = \frac{d}{dt} \left( \frac{\sigma_t^2 \bar{\sigma}_t^2}{\bar{\sigma}_t^2 + \sigma_t^2} \right) \quad (18d)$$

$$= \frac{d}{dt} \left( \frac{\sigma_t^2 (C - \sigma_t^2)}{C} \right) \quad (18e)$$

$$= \frac{1}{C} \frac{d}{dt} (C\sigma_t^2 - \sigma_t^4) \quad (18f)$$

$$= g^2(t) - \frac{2}{C} \sigma_t^2 g^2(t) \quad (18g)$$

$$= g^2(t) \left( 1 - \frac{2}{C} \sigma_t^2 \right). \quad (18h)$$

By substituting these into the definition of  $g^2(t)$ , we obtain

$$\frac{d\beta_t}{dt} - 2\beta_t \frac{d}{dt} \log \alpha_t = \frac{d}{dt} (\sigma_t^2 \alpha_t) - 2\sigma_t^2 \alpha_t \frac{d}{dt} \log \alpha_t \quad (19a)$$

$$= \alpha_t \frac{d\sigma_t^2}{dt} + \sigma_t^2 \frac{d\alpha_t}{dt} - 2\sigma_t^2 \alpha_t \left( \frac{1}{\alpha_t} \frac{d\alpha_t}{dt} \right) \quad (19b)$$

$$= \alpha_t g^2(t) - \sigma_t^2 \frac{d\alpha_t}{dt} \quad (19c)$$

$$= \left( 1 - \frac{\sigma_t^2}{C} \right) g^2(t) + \frac{\sigma_t^2}{C} g^2(t) \quad (19d)$$

$$= g^2(t), \quad (19e)$$

which completes the proof. □

## B Extended related works

### B.1 Diffusion models for inverse problems

In recent years, deep neural networks have gained significant attention for solving various inverse problems from different perspectives [Ongie et al., 2020, Chen et al., 2022]. Solving eq. (4) can be interpreted as sampling from the posterior distribution  $p(\mathbf{x} | \mathbf{y})$ , and generative models that support conditional generation are naturally suited to this task. Diffusion models, in particular, have emerged as SOTA tools for this purpose, thanks to their flexible mathematical formulation and expressive data priors [Daras et al., 2024]. The standard approach involves extending the diffusion process to sample from  $p(\mathbf{x}_0 | \mathbf{y})$  at  $t = 0$  by applying Bayes' Theorem. The conditional score function can be decomposed as  $\nabla_{\mathbf{x}_t} \log p(\mathbf{x}_t | \mathbf{y}) = \nabla_{\mathbf{x}_t} \log p(\mathbf{x}_t) + \nabla_{\mathbf{x}_t} \log p(\mathbf{y} | \mathbf{x}_t)$ , where the first term,  $\nabla_{\mathbf{x}_t} \log p(\mathbf{x}_t)$ , can be approximated using a pretrained score network  $\mathbf{s}_\theta(\mathbf{x}_t, t)$ , and the second term models the relationship between  $\mathbf{x}_t$  and the measurement  $\mathbf{y}$  [Song et al., 2021b, Dhariwal and Nichol, 2021]. This framework has spurred considerable progress in the field, with numerous successful methods emerging [Kawar et al., 2022, Chung et al., 2022, 2023a, Song et al., 2023a, Mardani et al., 2024, Chung et al., 2024]. Since this approach does not require retraining the score network for each specific problem, we refer to these methods as *unsupervised*.

Several works leverage the measurement system structure when applying pretrained diffusion models to inverse problems. Wang et al. [2023] (Denosing Diffusion Null-Space Models, DDNM) restrict updates during generation to the null space component of  $\mathbf{x}_t$ , keeping the range part fixed. Song

et al. [2023a] (Pseudoinverse-Guided Diffusion Models, IIGDM) approximate the likelihood score via a vector-Jacobian product, where the score network’s Jacobian is computed with automatic differentiation, and the vector reflects the range-nullspace decomposition. Garber and Tirer [2024] (Denosing Diffusion Models with Iteratively Preconditioned Guidance, DDPG) propose a method for interpolating between pseudoinverse-based and least-squares-based conditioning.

## B.2 Diffusion and Schrödinger bridges.

Diffusion models, while effective for high-quality image synthesis, are limited by the simplicity of Gaussian priors for  $p(\mathbf{x}_1)$ . Recent developments in *bridge models* [Särkkä and Solin, 2019] generalize the diffusion process by allowing  $p(\mathbf{x}_1)$  to be an arbitrary distribution. This is especially important in image restoration tasks, where paired samples  $(\mathbf{x}_0, \mathbf{x}_1)$ —clean and distorted images—are available. Bridge models aim to generate samples from the posterior  $p(\mathbf{x}_0 | \mathbf{x}_1)$  by initializing with a sample from  $p(\mathbf{x}_1)$  rather than Gaussian noise. While conditioning the standard score network on  $\mathbf{x}_1$  is a possible approach to achieve posterior sampling, it is often suboptimal [Batzolis et al., 2021].

Several methods have formulated the diffusion process as a stochastic bridge. Heng et al. [2021] propose a simulation-based algorithm using a fixed starting and ending point with an approximation of the true score. Liu et al. [2022] extend this with Doob’s h-transform [Doob, 1984] to bridge distributions. Simulation-free algorithms utilizing the h-transform are presented by Somnath et al. [2023] and Peluchetti [2022]. Delbracio and Milanfar [2023] construct a Brownian Bridge for direct restoration from  $\mathbf{x}_1$ . More recently, Zhou et al. [2024] introduce the DDBM framework, extending the VE and VP processes, while He et al. [2024] study DDBM within the consistency framework [Song et al., 2023b]. Zheng et al. [2025] link DDBM to Denosing Diffusion Implicit Models [Song et al., 2021a].

The Schrödinger Bridge (SB) problem [Schrödinger, 1932], which aligns distributions via constrained forward and reverse SDEs, has also been explored. De Bortoli et al. [2021] apply Iterative Proportional Fitting (IPF) to solve the SB problem. Liu et al. [2023] propose a tractable class of SBs, leading to a simulation-free algorithm (I2SB). Chung et al. [2023b] extend it with an additional guidance term. Shi et al. [2024] build on IPF and introduce Iterative Markovian Fitting for SB solutions.

In a related approach, Luo et al. [2023a] derive a scalar case of eq. (1) that incorporates the start and end points, termed the *mean-reverting* SDE (IR-SDE). Through specific parameterization, they show that its score function is analytically tractable, connecting to the Ornstein-Uhlenbeck (OU) process [Gillespie, 1996]. Yue et al. [2024] extend this work with a generalized OU process and Doob’s h-transform (GOUB). Further extensions include Luo et al. [2023b], who apply IR-SDE in latent spaces, and Welker et al. [2022] and Richter et al. [2023], who adapt similar processes for speech tasks. Recently, Zhu et al. [2025] unify GOUB and DDBM within the framework of stochastic optimal control.

## B.3 Baselines

### B.3.1 Unsupervised

We begin with describing the unsupervised baselines, which rely on solving the following scalar reverse equation:

$$d\mathbf{x}_t = [\mathbf{f}(\mathbf{x}_t, t) - g^2(t)\nabla_{\mathbf{x}_t} \log p(\mathbf{x}_t | \mathbf{y})]dt + g(t)d\bar{\mathbf{w}}_t, \quad (20)$$

where  $\mathbf{f}$  and  $g$  represent the drift and diffusion coefficients respectively, while  $\mathbf{y}$  is the conditioning variable representing measurements in the inverse problem context. Unsupervised diffusion-based methods rely on decomposing the score function with Bayes’ Theorem through  $\nabla_{\mathbf{x}_t} \log p(\mathbf{x}_t | \mathbf{y}) = \nabla_{\mathbf{x}_t} \log p(\mathbf{x}_t) + \nabla_{\mathbf{x}_t} \log p(\mathbf{y} | \mathbf{x}_t)$  and approximating  $\nabla_{\mathbf{x}_t} \log p(\mathbf{x}_t)$  with a pretrained  $\mathbf{s}_\theta(\mathbf{x}_t, t)$ , while proposing different approaches for  $\nabla_{\mathbf{x}_t} \log p(\mathbf{y} | \mathbf{x}_t)$ .

Diffusion Posterior Sampling (DPS, Chung et al. [2023a]) approximates  $p(\mathbf{y} | \mathbf{x}_t)$  with  $p(\mathbf{y} | \hat{\mathbf{x}}_0(\mathbf{x}_t))$ , where  $\hat{\mathbf{x}}_0(\mathbf{x}_t) = \mathbb{E}[\mathbf{x}_0 | \mathbf{x}_t] = \mathbf{x}_t + g^2(t)\nabla_{\mathbf{x}_t} \log p(\mathbf{x}_t)$  is the Tweedie’s formula [Robbins, 1992], giving an approximation of the denoised image at timestep  $t$ . Similarly,  $\nabla_{\mathbf{x}_t} \log p(\mathbf{x}_t)$  is also approximated with  $\mathbf{s}_\theta(\mathbf{x}_t, t)$  in this case.

Pseudoinverse-Guided Diffusion Model (IIGDM, Song et al. [2023a]) proposes to approximate the loglikelihood score with  $(\mathbf{y} - \mathbf{A}\hat{\mathbf{x}}_0(\mathbf{x}_t))^\top (r_t^2 \mathbf{A}\mathbf{A}^\top + \sigma_y^2 \mathbf{I})^{-1} \mathbf{A} \frac{\partial \hat{\mathbf{x}}_0(\mathbf{x}_t)}{\partial \mathbf{x}_t}$ , where  $\sigma_y^2 \mathbf{I}$  is the measurement

system covariance and  $r_t^2$  is a time-dependent term that should depend on the data (Appendix A.3., Song et al. [2023a]). Using automatic differentiation, one can compute  $\frac{\partial \hat{\mathbf{x}}_0(\mathbf{x}_t)}{\partial \mathbf{x}_t}$ . By combining it with the other terms, the entire approximation can be efficiently computed as a vector-Jacobian product.

In their basic formulation, Denoising Diffusion Null-space Models (DDNM, Wang et al. [2023]) rely on approximating  $p(\mathbf{x}_{t-1} | \mathbf{x}_t, \mathbf{y})$  using the following update rule:

$$\mathbf{x}_{t-1} = \frac{\sqrt{\bar{\alpha}_{t-1}}\beta_t}{1 - \bar{\alpha}_t} \hat{\mathbf{x}}_0(\mathbf{x}_t, \mathbf{y}) + \frac{\sqrt{\alpha_t}(1 - \bar{\alpha}_{t-1})}{1 - \bar{\alpha}_t} \mathbf{x}_t + \sigma_t \epsilon, \quad (21)$$

where  $\epsilon \sim \mathcal{N}(\mathbf{0}, \mathbf{I})$  and  $\alpha_t, \beta_t$  follow the notation from the original work. This rule utilizes the range-nullspace decomposition via  $\hat{\mathbf{x}}_0(\mathbf{x}_t, \mathbf{y}) = \mathbf{A}^+ \mathbf{y} + (\mathbf{I} - \mathbf{A}^+ \mathbf{A}) \hat{\mathbf{x}}_0(\mathbf{x}_t)$ , which preserves the true range space component, while updating the null space part with Tweedie’s estimate.

### B.3.2 Supervised

We proceed with a description of baseline supervised bridge methods. All of these approaches assume a stochastic process conditioned on both the starting and ending point with the following forward and reverse equations:

$$d\mathbf{x}_t = \mathbf{f}(\mathbf{x}_t, \mathbf{x}_T, t, T)dt + g(t)d\mathbf{w}_t, \quad (22a)$$

$$d\mathbf{x}_t = \mathbf{f}'(\mathbf{x}_t, \mathbf{x}_T, t, T)dt + g(t)d\bar{\mathbf{w}}_t, \quad (22b)$$

where  $\mathbf{f}, \mathbf{f}'$  represent general drift coefficients respectively for the forward and reverse equation,  $g$  is the diffusion coefficient and  $\mathbf{x}_T$  represents the endpoint for the initial  $\mathbf{x}_0$ .

Image-to-Image Schrodinger Bridges (I2SB, Liu et al. [2023]) formulate the distribution of  $\mathbf{x}_t$ , given starting and ending points  $\mathbf{x}_0, \mathbf{x}_T$ , as  $p(\mathbf{x}_t | \mathbf{x}_0, \mathbf{x}_T) = \mathcal{N}(\frac{\bar{\sigma}_t^2}{\bar{\sigma}_t^2 + \sigma_t^2} \mathbf{x}_0 + \frac{\sigma_t^2}{\bar{\sigma}_t^2 + \sigma_t^2} \mathbf{x}_T, \frac{\sigma_t^2 \bar{\sigma}_t^2}{\bar{\sigma}_t^2 + \sigma_t^2} \mathbf{I})$ , where  $\sigma_t^2 = \int_0^t g^2(\tau)d\tau, \bar{\sigma}_t^2 = \int_t^1 g^2(\tau)d\tau$  and show its equivalence to DDPM posterior sampling [Ho et al., 2020].

Image Restoration SDE (IR-SDE, Luo et al. [2023a]) is based on formulating the forward and reverse equations as

$$d\mathbf{x}_t = \theta_t(\mathbf{x}_T - \mathbf{x}_t)dt + \sigma(t)d\mathbf{w}_t, \quad (23a)$$

$$d\mathbf{x}_t = [\theta_t(\mathbf{x}_T - \mathbf{x}_t) - \sigma^2(t)\nabla_{\mathbf{x}_t} \log p(\mathbf{x}_t)]dt + \sigma(t)d\bar{\mathbf{w}}_t, \quad (23b)$$

where  $\theta_t = \frac{\sigma_t^2}{\lambda^2}, \bar{\theta}_t = \int_0^t \theta_\tau d\tau$  and  $\lambda$  is a predefined constant. At  $t = 1$ , IR-SDE arrives at a Gaussian distribution (with non-zero covariance) centered at  $\mathbf{x}_T$ .

Generalized Ornstein-Uhlenbeck Bridges (GOUB, Yue et al. [2024]) show IR-SDE as a special case of their framework by incorporating the Doob’s h-transform [Doob, 1984], which pulls the process towards the desired endpoint. Formally, it is defined as  $\mathbf{h}(\mathbf{x}_t, t, \mathbf{x}_T, T) = \nabla_{\mathbf{x}_t} \log p(\mathbf{x}_T | \mathbf{x}_t)$  and incorporated into the forward and reverse equations:

$$d\mathbf{x}_t = \left( (\theta_t + g^2(t) \frac{e^{-2\bar{\theta}_{t:T}}}{\bar{\sigma}_{t:T}^2})(\mathbf{x}_T - \mathbf{x}_t) \right) dt + g(t)d\mathbf{w}_t, \quad (24a)$$

$$d\mathbf{x}_t = \left( (\theta_t + g^2(t) \frac{e^{-2\bar{\theta}_{t:T}}}{\bar{\sigma}_{t:T}^2})(\mathbf{x}_T - \mathbf{x}_t) - g^2(t)\nabla_{\mathbf{x}_t} \log p(\mathbf{x}_t | \mathbf{x}_T) \right) dt + g(t)d\bar{\mathbf{w}}_t, \quad (24b)$$

where  $\theta_t = \frac{g^2(t)}{2\lambda^2}, \bar{\theta}_{s:t} = \int_s^t \theta_\tau d\tau, \bar{\sigma}_{s:t}^2 = \frac{g^2(t)}{2\theta_t}(1 - e^{-2\bar{\theta}_{s:t}})$  for a predefined constant  $\lambda$ .

Denoising Diffusion Bridge Model, (DDBM, Zhou et al. [2024]) also utilize the h-transform, but instead show how to adapt prior unconditional processes, which map images to Gaussian noise, to construct a bridge between arbitrary distributions given paired data:

$$d\mathbf{x}_t = [\mathbf{f}(\mathbf{x}_t, t) + g^2(t)\mathbf{h}(\mathbf{x}_t, t, \mathbf{x}_T, T)]dt + g(t)d\mathbf{w}_t, \quad (25a)$$

$$d\mathbf{x}_t = [\mathbf{f}(\mathbf{x}_t, t) - g^2(t)(\nabla_{\mathbf{x}_t} \log p(\mathbf{x}_t | \mathbf{x}_T) - \mathbf{h}(\mathbf{x}_t, t, \mathbf{x}_T, T))]dt + g(t)d\bar{\mathbf{w}}_t, \quad (25b)$$

where  $\mathbf{f}(\mathbf{x}_t, t), g(t)$  follow the original image-to-noise process.

## C Extended methodology

### C.1 Network parameterization

In a scalar setting, various reparameterizations of the score function were shown to provide different trade-offs in the final performance [Ho et al., 2020]. For example, the network could instead predict the added noise directly, which is bijectively obtained from the score. As these reparameterizations are related through simple scalar functions, one can choose them freely without additional considerations. In the matrix-valued setting, however, the choice of a parameterization is more subtle. In this case, observe that  $\nabla_{\mathbf{x}_t} \log p(\mathbf{x}_t) = -\Sigma_t^{-1}(\mathbf{x}_t - \mathbf{H}_t \mathbb{E}[\mathbf{x}_0 | \mathbf{x}_t])$ . Training a score-prediction model hence requires access to the inverse of  $\Sigma_t$ , which may in general be costly to obtain. By properly choosing the form of  $\gamma_t$  and  $\beta_t$ , one can show that  $\mathbf{G}_t \mathbf{G}_t^\top \nabla_{\mathbf{x}_t} \log p(\mathbf{x}_t) = (f_t \mathbf{I} - 2\mathbf{F}_t)(\mathbf{H}_t \mathbb{E}[\mathbf{x}_0 | \mathbf{x}_t] - \mathbf{x}_t)$  for some function  $f_t$ , *i.e.*, an  $\mathbf{x}_0$ -prediction model alleviates the need for computing  $\Sigma_t^{-1}$ . Therefore, we treat this parameterization as the default one for SDB.

### C.2 Nonlinear measurement systems

While not the focus of this work, inverse problems with nonlinear system response  $\mathbf{A}$  may also be considered, *e.g.*, in the problem of GAN inversion [Creswell and Bharath, 2018]. Assuming that  $\mathbf{A}$  is differentiable, it may be locally linearized using Taylor expansion as  $\mathbf{A}(\mathbf{x}) \approx \mathbf{A}(\mathbf{x}_0) + \mathbf{J}_{\mathbf{A}} \mathbf{x}_0 (\mathbf{x} - \mathbf{x}_0)$  around some point  $\mathbf{x}_0$ , where  $\mathbf{J}_{\mathbf{A}}$  is the Jacobian of  $\mathbf{A}$ . To adapt SDB to such cases, one can use  $\mathbf{J}_{\mathbf{A}}$  as a local linear approximation of  $\mathbf{A}$  and treat it instead as the system response matrix. We consider further study of such models as future work.

### C.3 Pseudocode

We provide pseudocode for SDB for both training and Euler-Maruyama sampling in algorithm 1 and algorithm 2 respectively.

---

#### Algorithm 1 SDB Training

---

**Require:**  $p(\mathbf{x}_0), p(t), \mathbf{A}, \mathbf{A}^+, \Sigma^{1/2}, \alpha_t, \beta_t, \gamma_t, \mathbf{D}\theta$

- 1: **for** each iteration **do**
- 2:    $\mathbf{x} \sim p(\mathbf{x})$
- 3:    $t \sim p(t)$
- 4:    $\epsilon \sim \mathcal{N}(\mathbf{0}, \mathbf{I}) \in \mathbb{R}^m$
- 5:    $\epsilon' \sim \mathcal{N}(\mathbf{0}, \mathbf{I}) \in \mathbb{R}^d$
- 6:    $\mathbf{x}_t \leftarrow [\mathbf{A}^+ \mathbf{A} + \alpha_t (\mathbf{I} - \mathbf{A}^+ \mathbf{A})] \mathbf{x} + \gamma_t^{\frac{1}{2}} \mathbf{A}^+ \Sigma^{\frac{1}{2}} \epsilon + \beta_t^{\frac{1}{2}} (\mathbf{I} - \mathbf{A}^+ \mathbf{A}) \epsilon'$
- 7:    $L_\theta \leftarrow \|\mathbf{D}\theta(\mathbf{x}_t, t) - \mathbf{x}\|_1$
- 8:    $\theta \leftarrow \text{optimizer}(\nabla_\theta L_\theta)$
- 9: **end for**
- 10: **return**  $\theta$

---

## D Experimental setup

### D.1 Training hyperparameters

We follow the training procedure proposed by Luo et al. [2023a], using the ADAM optimizer [Kingma and Ba, 2015] with an initial learning rate of  $1 \times 10^{-4}$ , no weight decay, and  $(\beta_1, \beta_2) = (0.9, 0.99)$ . A multi-step learning rate scheduler is applied, halving the learning rate at the 36th, 60th, 72nd, and 90th epochs, as in the original work. All methods are trained using the  $\ell_1$  loss function with a batch size of 8. To ensure fairness across methods, we evaluate each model every 16 epochs and report the performance of the best checkpoint, rather than relying solely on the final one.

### D.2 Computational requirements

All experiments were conducted on a cluster of NVIDIA A100 GPUs, with each method trained using a single GPU. The approximate training times for each task are as follows: 4 hours for super-resolution, 24 hours for MRI reconstruction, 48 hours for CT reconstruction, and 72 hours for inpainting.

---

**Algorithm 2** SDB Sampling (Euler-Maruyama)
 

---

**Require:**  $N, \mathbf{A}, \mathbf{A}^+, \Sigma^{1/2}, \alpha_t, \beta_t, \gamma_t, \mathbf{H}_t, \mathbf{F}_t, D_{\theta}, \mathbf{y}$ 

- 1:  $t \leftarrow 1$
  - 2:  $\Delta t \leftarrow 1/N$
  - 3:  $\epsilon' \sim \mathcal{N}(\mathbf{0}, \mathbf{I}) \in \mathbb{R}^d$
  - 4:  $\hat{\mathbf{x}} \leftarrow \mathbf{A}^+ \mathbf{y}$
  - 5:  $\mathbf{x}_t \leftarrow \hat{\mathbf{x}} + \beta_t^{1/2} (\mathbf{I} - \mathbf{A}^+ \mathbf{A}) \epsilon'$
  - 6: **for**  $i \in \{1, \dots, N\}$  **do**
  - 7:    $\epsilon \sim \mathcal{N}(\mathbf{0}, \mathbf{I}) \in \mathbb{R}^m$
  - 8:    $\epsilon' \sim \mathcal{N}(\mathbf{0}, \mathbf{I}) \in \mathbb{R}^d$
  - 9:    $\mathbf{x}_{t-\Delta t} \leftarrow \mathbf{x}_t + \Delta t [(f_t \mathbf{I} - 2\mathbf{F}_t)(\mathbf{H}_t D_{\theta}(\mathbf{x}_t, t) - \mathbf{x}_t) - \mathbf{F}_t \mathbf{x}_t] + \Delta t^{1/2} \left[ \left( \frac{d\gamma_t}{dt} \right)^{1/2} \mathbf{A}^+ \Sigma^{1/2} \epsilon + \left( \frac{d\beta_t}{dt} - 2\beta_t \frac{d}{dt} \log \alpha_t \right)^{1/2} (\mathbf{I} - \mathbf{A}^+ \mathbf{A}) \epsilon' \right]$
  - 10:    $t \leftarrow t - \Delta t$
  - 11: **end for**
  - 12: **return**  $\mathbf{x}_0$
- 

## E Additional experimental results

### E.1 Evaluation under a misspecified model (CT reconstruction)

Figure 4 presents the results of an analogous analysis of performance of bridge methods under a misspecified model (here in CT reconstruction task), where the first part of the experiment considers the default setting of  $\sigma_1^2$  with increasing  $\tau$ , while the second part shows the results for  $\tau = 3.6$  and increasing  $\sigma_1^2$ . In a similar manner to section 5.2, all SDB variants achieve a clear advantage over other bridge methods when the system’s parameters are perturbed.

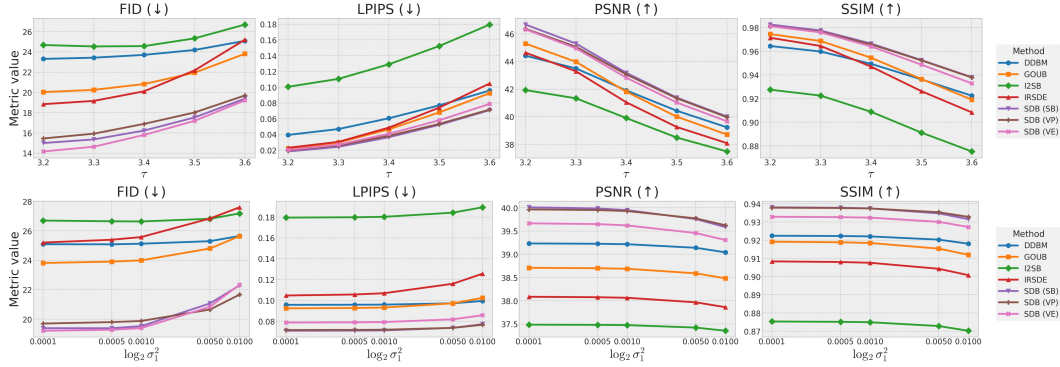


Figure 4: Quantitative comparison of SDB (SB) with other bridge methods in a misspecified CT reconstruction setting. The **top** row evaluates bridges trained with  $\tau = 3.2$ ,  $\sigma_1^2 = 0.0001$  on data generated from systems with increasing  $\tau$ . The **bottom** row evaluates performance on data with  $\tau = 3.6$  and increasing  $\sigma_1^2$ . Perturbing the original system makes the problem harder in both cases.

### E.2 Hyperparameter analysis

We conduct an ablation study to analyze the sensitivity of SDB to its hyperparameters. Following prior works [Zhou et al., 2024], our stochastic process is undefined at  $t = 1$ , requiring sampling to begin at  $t = 1 - \epsilon_1$  for some  $\epsilon_1 > 0$ . Similarly, we terminate sampling at  $t = \epsilon_2$ , where  $\epsilon_2 > 0$ . For SDB (VP) and SDB (VE),  $\epsilon_1$  and  $\epsilon_2$  are the only hyperparameters. In contrast, SDB (SB) includes an additional design choice: the shape of the null-space diffusion coefficient  $g(t)$ . We parameterize it as

$$g^2(t) = \mathbb{1}_{t \leq 0.5} \hat{g}(t) + \mathbb{1}_{t > 0.5} \hat{g}(1 - t)$$

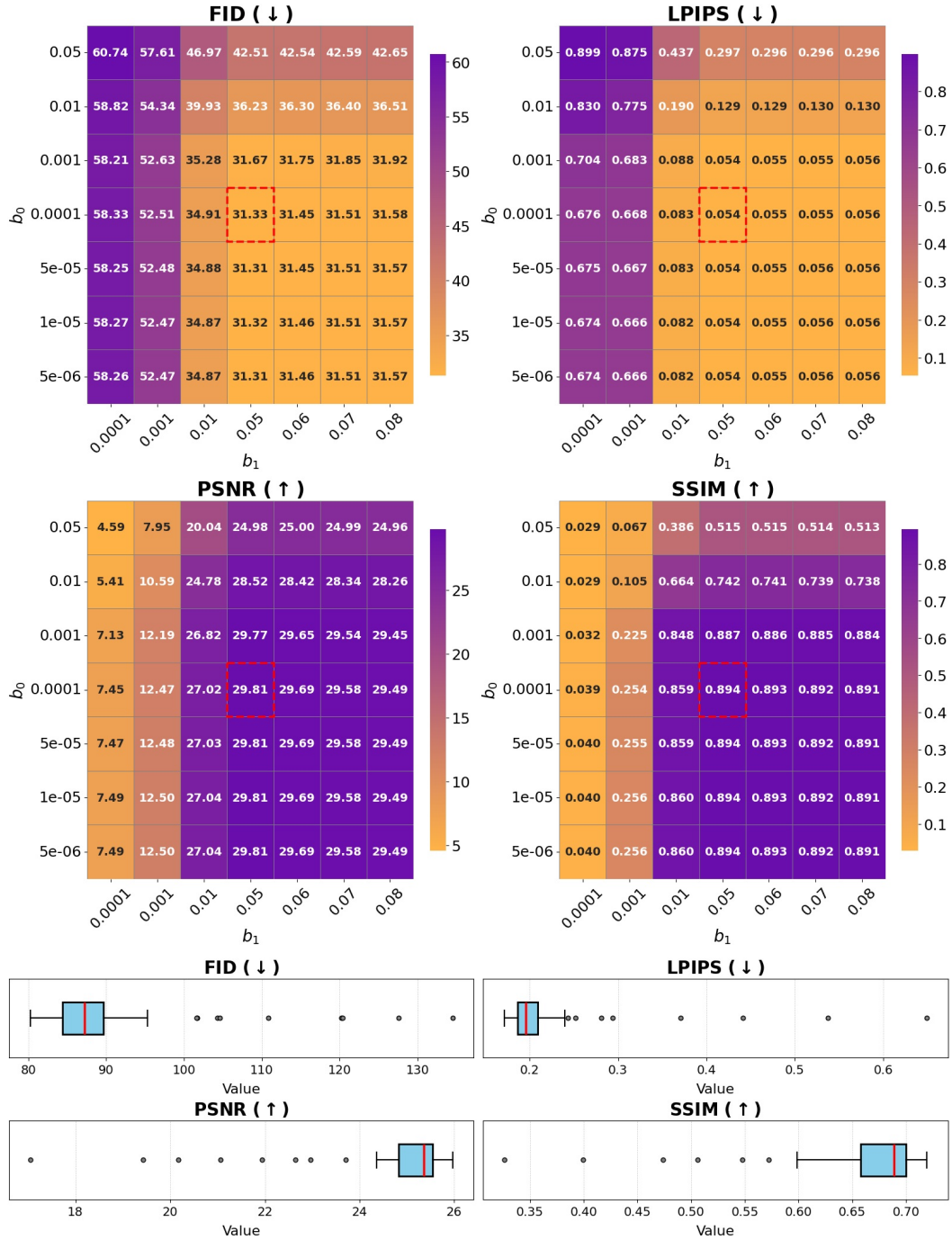


Figure 5: **Top:** Performance heatmaps for MRI reconstruction under varying  $(\epsilon_1, \epsilon_2)$ , using the optimal  $(b_0, b_1)$  configuration. The red box highlights the LPIPS-optimal setting. **Bottom:** Boxplots showing the best achievable performance across 64  $(b_0, b_1)$  pairs on the superresolution task, where  $(\epsilon_1, \epsilon_2)$  are tuned separately for each  $(b_0, b_1)$  pair.

where  $\hat{g}(t) = (\sqrt{b_0} + t(\sqrt{b_1} - \sqrt{b_0}))^2$ , which is a continuous version of the coefficient proposed by Liu et al. [2023]. This introduces two additional hyperparameters,  $b_0, b_1 > 0$ . In the remainder of this section, we focus on SDB (SB), noting that we observed qualitatively similar trends for the VP and VE variants.

We first examine how the choice of  $\epsilon_1$  and  $\epsilon_2$  influences the optimal configuration of  $(b_0, b_1)$  for SDB (SB) in the MRI reconstruction task. Figure 5 (top) shows the performance trend when varying  $(\epsilon_1, \epsilon_2)$ . We observe a simple and stable relationship with performance, where  $\epsilon_1$  has a stronger influence than  $\epsilon_2$ . Moreover, a broad plateau emerges, allowing for easy tuning. We also highlight the best configuration in terms of LPIPS, which lies close to the optimal Pareto frontier in this setting.

Next, we analyze the stability of SDB (SB) across different  $(b_0, b_1)$  configurations. Since these values determine the shape of the variance function, the optimal  $\epsilon_1, \epsilon_2$  may differ across  $(b_0, b_1)$  pairs. Figure 5 (bottom) presents boxplots of the best performance for 64 configurations of  $(b_0, b_1)$  on the superresolution task. For each pair, we use grid search to identify the best  $\epsilon_1, \epsilon_2$  values, leveraging the small size of the DIV2K dataset. The results reveal strong stability, with performance concentrated around the best observed value and only a few outliers.

## F Broader impact

By incorporating measurement system parameters into its SDE, SDB offers positive societal impacts by enabling more accurate and efficient reconstructions in critical applications such as medical imaging, remote sensing, and scientific inverse problems, thereby supporting improved diagnostics, sustainability, and broader accessibility. However, it also poses potential negative societal risks, including misuse for surveillance or de-anonymization, amplification of bias from flawed measurement models, and overreliance on plausible but incorrect outputs in high-stakes domains. Additionally, the method could be repurposed for generating deceptive content from limited data. However, SDB and prior bridge methods have not been demonstrated at industry-scale deployment levels, and in practice, they are typically suited for problem-specific applications rather than large-scale settings with vast amounts of data. This limits their potential for misuse in broader societal contexts.

## G Additional visual results

We provide additional qualitative samples for inpainting (fig. 6), superresolution (fig. 7), MRI reconstruction (fig. 8) and CT reconstruction (fig. 9).

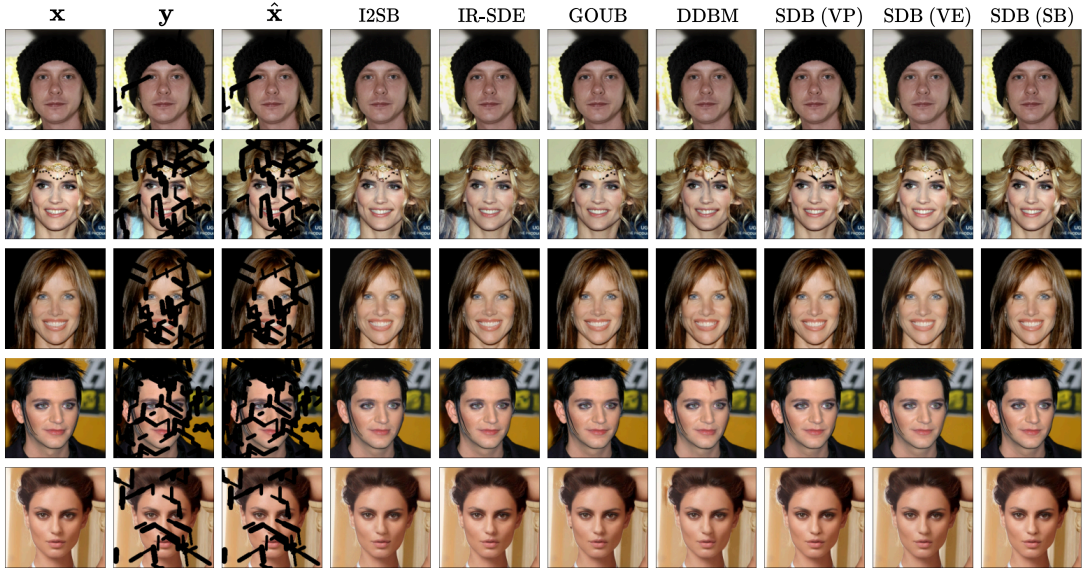


Figure 6: Qualitative comparison of SDB variants with the best-performing baselines (bridge methods). Rows depict the results for inpainting.

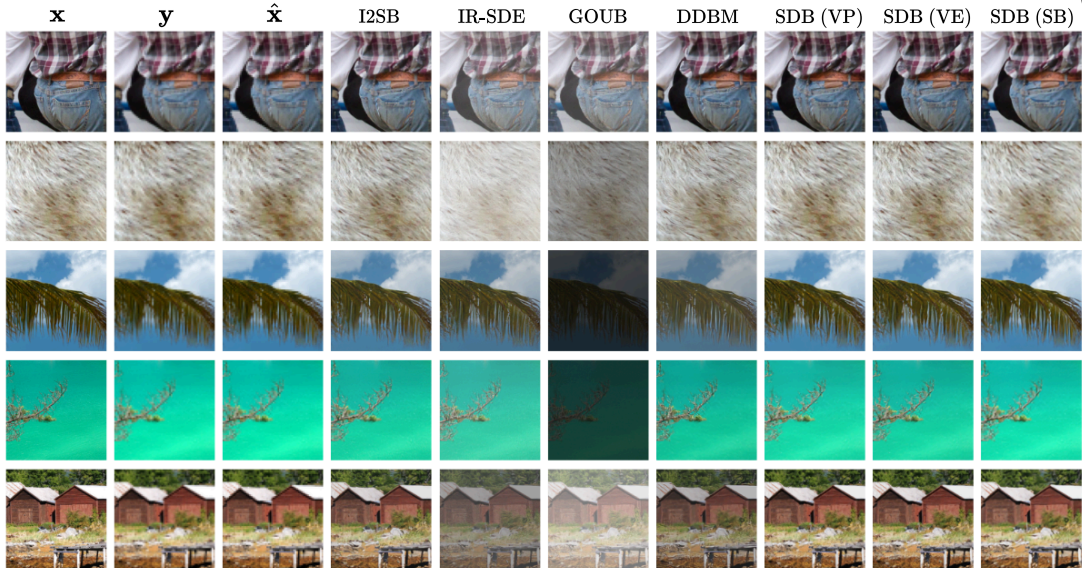


Figure 7: Qualitative comparison of SDB variants with the best-performing baselines (bridge methods). Rows depict the results for superresolution.

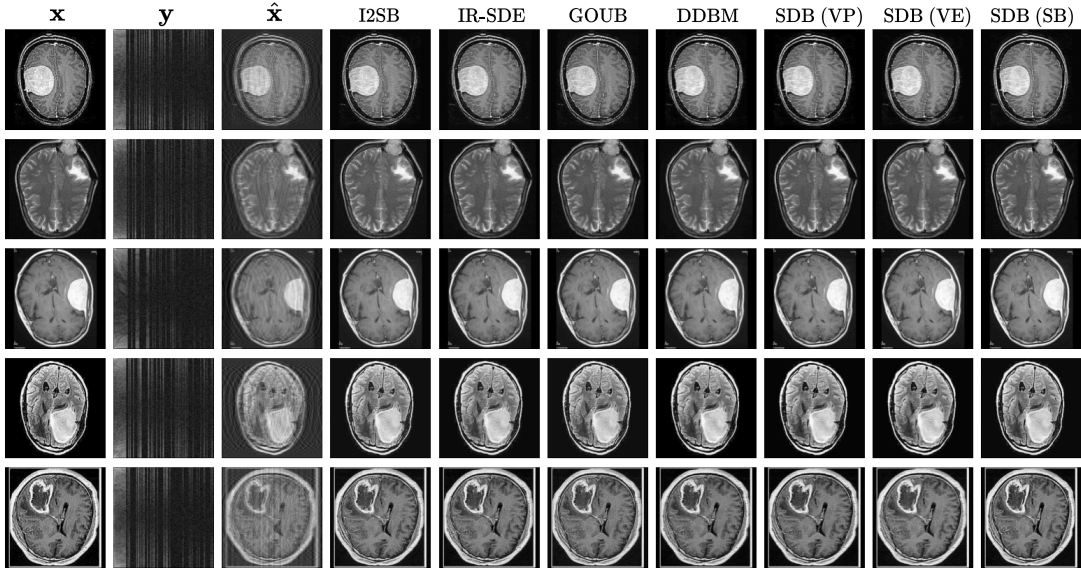


Figure 8: Qualitative comparison of SDB variants with the best-performing baselines (bridge methods). Rows depict the results for MRI reconstruction.

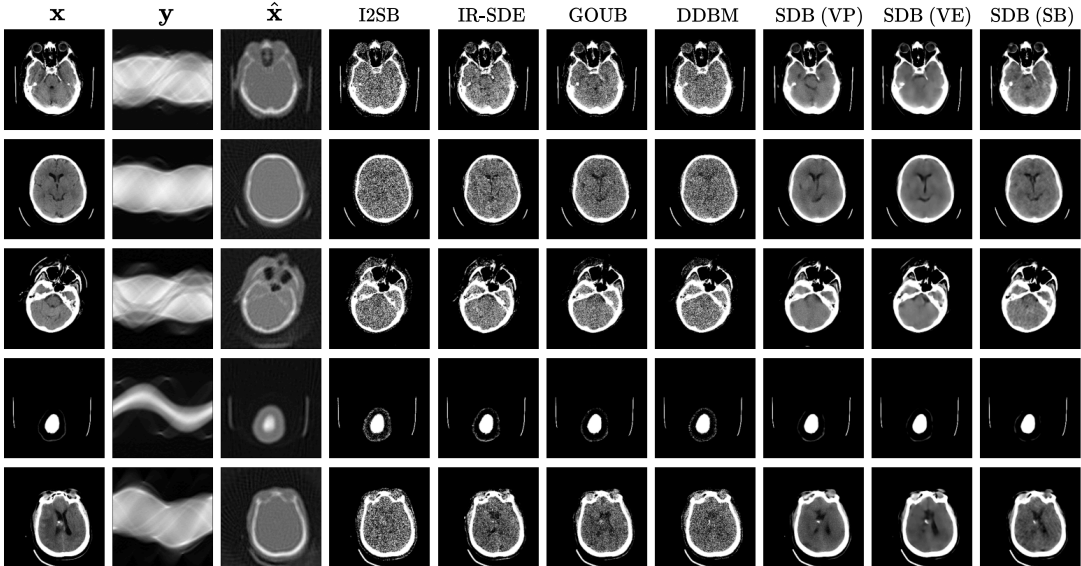


Figure 9: Qualitative comparison of SDB variants with the best-performing baselines (bridge methods). Rows depict the results for CT reconstruction.